










# A mitochondrial RNA processing protein mediates plant immunity to a broad spectrum of pathogens by modulating the mitochondrial oxidative burst

Yang Yang <sup>1</sup>, Yan Zhao <sup>1</sup>, Yingqi Zhang <sup>1</sup>, Lihua Niu <sup>1</sup>, Wanyue Li <sup>1</sup>, Wenqin Lu <sup>2</sup>, Jinfang Li <sup>2</sup>, Patrick Schäfer <sup>3</sup>, Yuling Meng <sup>1</sup> and Weixing Shan <sup>1,\*†</sup>

- 1 State Key Laboratory of Crop Stress Biology in Arid Areas and College of Agronomy, Northwest A&F University, Yangling 712100, China
- 2 State Key Laboratory of Crop Stress Biology in Arid Areas and College of Plant Protection, Northwest A&F University, Yangling 712100, China
- 3 Institute of Molecular Botany, Ulm University, Ulm 89069, Germany

\*Author for correspondence: wxshan@nwafu.edu.cn

†Senior author

W.S. and Y.Y. conceived the research. Y.Y. performed most of the experiments. W.Q.L. and Y.Z. conducted SA treatment assays. W.Y.L., Y.Q.Z., L.H.N., and J.F.L. conducted *P. infestans* and *B. cinerea* inoculation assays. Y.Y., Y.L.M., Y.Z., P.S., and W.S. analyzed the data. Y.Y. and W.S. wrote the manuscript with contribution from all authors.

The author responsible for distribution of materials integral to the findings presented in this article in accordance with the policy described in the Instructions for Authors (<https://academic.oup.com/plcell>) is Weixing Shan (wxshan@nwafu.edu.cn).

## Abstract

Mitochondrial function depends on the RNA processing of mitochondrial gene transcripts by nucleus-encoded proteins. This posttranscriptional processing involves the large group of nuclear-encoded pentatricopeptide repeat (PPR) proteins. Mitochondrial processes represent a crucial part in animal immunity, but whether mitochondria play similar roles in plants remains unclear. Here, we report the identification of RESISTANCE TO PHYTOPHTHORA PARASITICA 7 (AtRTP7), a P-type PPR protein, in *Arabidopsis thaliana* and its conserved function in immunity to diverse pathogens across distantly related plant species. RTP7 affects the levels of mitochondrial reactive oxygen species (mROS) by participating in RNA splicing of *nad7*, which encodes a critical subunit of the mitochondrial respiratory chain Complex I, the largest of the four major components of the mitochondrial oxidative phosphorylation system. The enhanced resistance of *rtp7* plants to *Phytophthora parasitica* is dependent on an elevated mROS burst, but might be independent from the ROS burst associated with plasma membrane-localized NADPH oxidases. Our study reveals the immune function of RTP7 and the defective processing of Complex I subunits in *rtp7* plants resulted in enhanced resistance to both biotrophic and necrotrophic pathogens without affecting overall plant development.

## Introduction

Mitochondria are semiautonomous organelles with various functions ranging from primary metabolism to oxidative phosphorylation (Meyer et al., 2019). The posttranscriptional modifications of mitochondria-encoded genes require nucleus-encoded proteins (Braun et al., 2014). Pentatricopeptide repeat

(PPR) proteins are nucleus-encoded proteins with hundreds of members in land plants and PPR proteins mainly participate in RNA processing in mitochondria and chloroplasts (Barkan and Small, 2014). The posttranscriptional modifications mediated by PPR proteins are critical for the normal functions of mitochondria-encoded genes.

## IN A NUTSHELL

**Background:** Diseases are major constraints for sustainable crop production. *Phytophthora* pathogens are notorious for their ability to overcome host genotype-specific resistance. Although pathogen effector recognition-based disease resistance is well documented, little is known about plant susceptibility. Developing novel strategies based on understanding plant susceptibility is an alternative strategy to improve crop disease resistance. A forward genetics approach was employed to understand plant susceptibility to *Phytophthora* pathogens in *Arabidopsis thaliana*, leading to the identification of the mitochondrial RNA processing factor RESISTANCE TO PHYTOPHTHORA PARASITICA 7 (AtRTP7). Mitochondria contain many core subunits of complexes in the electron transport chain (ETC) required for energy production. The mitochondrial transcripts encoding ETC components are processed via RNA splicing and RNA editing.

**Question:** How does the mitochondrial RNA processing factor RTP7 mediate plant susceptibility? Is the *rtp7*-mediated resistance effective against a broad spectrum of pathogens? We addressed these using a range of approaches.

**Findings:** We found that RTP7 encodes a pentatricopeptide repeat protein in *A. thaliana* and negatively regulates plant immunity to the oomycete *Phytophthora parasitica* and fungal and bacterial pathogens. RTP7 participates in intron splicing of *nad7*, which encodes a core subunit of complexes in the ETC, and regulates mitochondrial reactive oxygen species (mROS) accumulation, which is responsive to pathogen infection. By using ROS scavengers to reduce mROS levels and by generating double and triple mutants of *rtp7* with the plasma membrane-localized NADPH oxidases *rbohD* and *rbohF*, we showed that the broad-spectrum disease resistance of *rtp7* plants is mediated by enhanced mROS, but not the ROS produced by host plant plasma membrane-associated RBOHD and RBOHF.

**Next steps:** We showed a close link between mitochondrial RNA processing in regulating mROS bursts and plant disease resistance against a broad spectrum of pathogens. The conserved immune function of RTP7 reveals its great potential in engineering novel disease resistance in crops against diverse pathogens in the future.

PPR proteins usually contain tandem arrays of approximately 35 amino acid repeat motif called the PPR motif. There are three types of PPR motifs: the typical 35 amino acid PPR repeat (P motif), 35–36 amino acid L motif, and 31 amino acid S motif (Barkan and Small, 2014). There are two subfamilies of PPR proteins: P and PLS (Barkan and Small, 2014). Normally, P-type proteins only contain PPR motifs, but PLS-type proteins also contain other types of domains in the C-terminal region (Barkan and Small, 2014).

Many P-type PPR proteins function in RNA splicing of mitochondrial group II introns that lack the capability to self-splice (Bonen, 2008; Barkan and Small, 2014; Brown et al., 2014). PLS-type proteins typically function in cytidine-to-uridine RNA editing (Barkan and Small, 2014), which is the most common type of editing in mitochondria and usually occurs on the first or second positions of triplet codons (Gray and Covello, 1993; Takenaka et al., 2013; Barkan and Small, 2014; Shikanai, 2015; Yan et al., 2017).

While mitochondria and chloroplast are important organelles in plant immunity (Huang et al., 2013; Serrano et al., 2016), there are only very few reports on the immune function of PPR proteins (Zhu et al., 2014; Qiu et al., 2021) and the role of RNA editing related factors in regulation of plant immunity. For instance, *Arabidopsis thaliana* OVEREXPRESSION OF CATIONIC PEROXIDASE 3 (OCP3) functions in the RNA editing of transcripts of the chloroplast gene *ndhB* and plant

immunity to the necrotrophic pathogen *Plectosphaerella cucumerina* (Garcia-Andrade et al., 2013).

In mitochondria, the NADH-ubiquinone oxidoreductase complex (Complex I) is the main point through which electrons enter the respiratory electron transport chain (ETC; Møller, 2001). Nine of the Complex I subunits (*nad1*, *nad2*, *nad3*, *nad4*, *nad4L*, *nad5*, *nad6*, *nad7*, and *nad9*) are encoded by the mitochondrial genome, and all of them are core subunits of Complex I (Klusich et al., 2021). Normal RNA modification is required and crucial for the functions of these nine proteins in oxidative phosphorylation (Unsel et al., 1997; Barkan and Small, 2014).

Complex I is one of the major sites of reactive oxygen species (ROS) production (Møller, 2001). Mitochondrial ROS (mROS) have been shown to regulate a variety of biological processes in animals including innate and adaptive immune responses (Chandel, 2014; Chen et al., 2018). In plants, the function of RNA processing of respiratory complexes in immunity is not well understood but may affect the activation of ROS bursts as part of an immunity-pertinent programmed cell death response (Yao and Greenberg, 2006; Amirsadeghi et al., 2007; Cvetkovska and Vanlerberghe, 2012; Colombatti et al., 2014).

*Phytophthora* species belong to a unique group of eukaryotic microorganisms called oomycetes that are phylogenetically distinct from true fungi. Nearly, all 120 *Phytophthora* species are plant pathogens on a wide range of host plants,

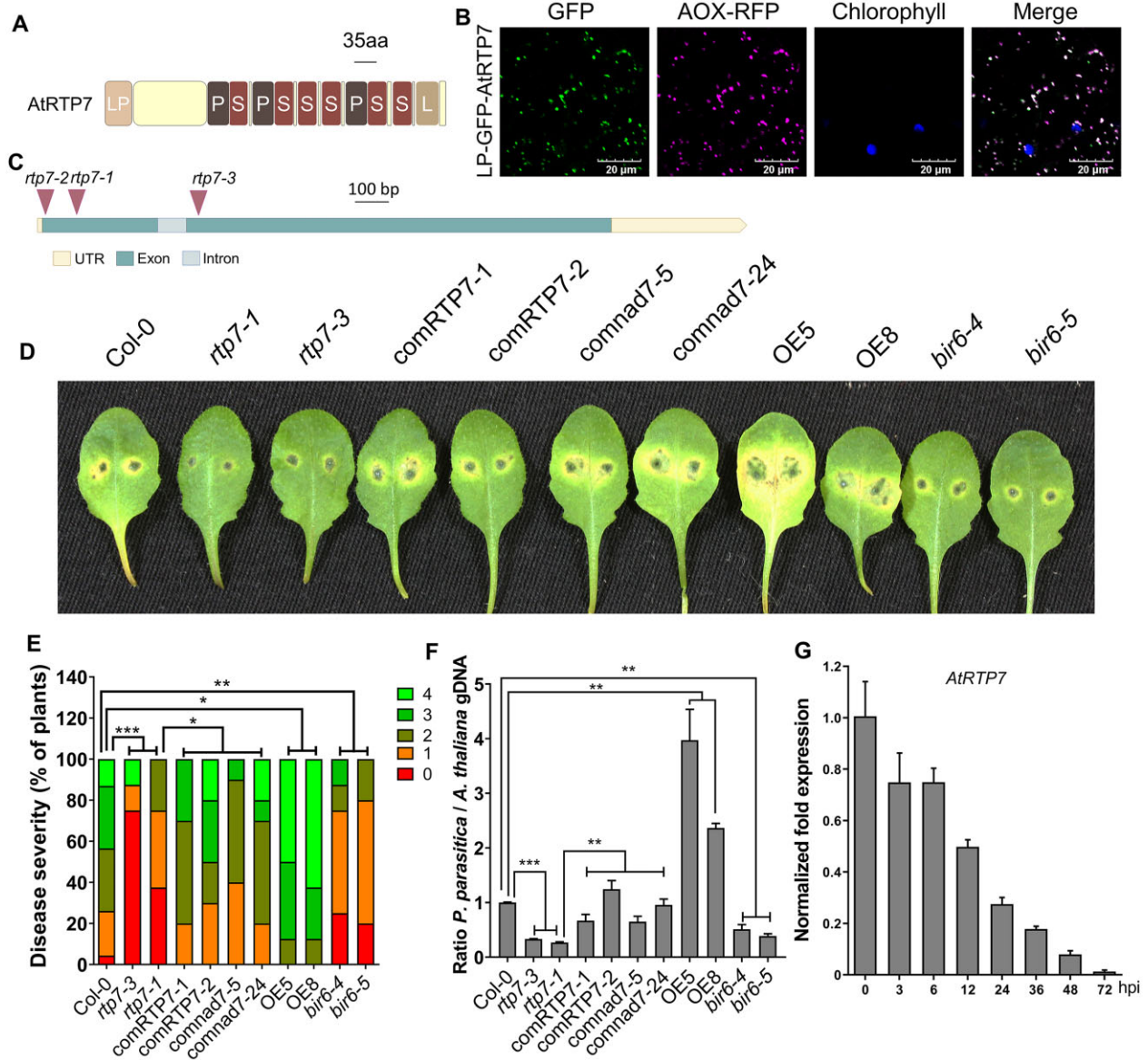


**Figure 1** *AtRTP7* encodes a mitochondrial P-type PPR protein and negatively affects *A. thaliana* immunity to *P. parasitica*. A, *AtRTP7* encodes a P-type PPR protein with 10 PPR motifs. P, P motif; L, L motif; S, S motif. B, The subcellular localization of LP-GFP-*AtRTP7*. The subcellular localization of the fusion protein in *N. benthamiana* leaves was determined using confocal microscopy at 3-day post agroinfiltration. AOX-RFP was used as a mitochondrial marker. Chlorophyll fluorescence was used as a chloroplast marker. Similar results were observed in three different *N. benthamiana* leaves. C, Schematic view of the T-DNA insertion sites of the three *rtp7* mutants. The T-DNA of *rtp7-1* and *rtp7-2* are inserted in the first exon of *AtRTP7*, and the T-DNA of *rtp7-3* mutant is inserted in the second exon. D–F, Images (D) and disease severity assessment (E) and *P. parasitica* biomass (F) of *P. parasitica* lesions in the *rtp7* mutants, *AtRTP7*-OE5 and OE8, *AtRTP7*-complementation lines (*comRTP7-1* and *comRTP7-2*), *nad7*-complementation lines (*comnad7-5* and *comnad7-24*), and *bir6* mutants. Images were taken at ~40 h after inoculation with *P. parasitica* zoospores. Biomass is presented as the mean  $\pm$  SE (standard error of mean) of at least three repeats (four inoculated leaves from different plants were gathered together as one repeat). Statistical significance was assessed by Student's *t* test for biomass analysis and Wilcoxon–Mann–Whitney test for disease severity assessment. \**P* < 0.05, \*\**P* < 0.01, and \*\*\**P* < 0.001. Similar results were observed in five independent experiments. G, The expression pattern of *AtRTP7* during *P. parasitica* infection. Total RNA was extracted from leaves infected with *P. parasitica* zoospores at 3, 6, 12, 24, 36, 48, and 72 hpi. The expression level was determined by RT-qPCR, with the *A. thaliana* *UBC9* gene as an internal control. Results are presented as the mean  $\pm$  SE of three repeats (two inoculated leaves from different plants were gathered together as one repeat for one time point). Similar results were observed in two independent experiments.

including the notorious potato (*Solanum tuberosum*) late blight pathogen *Phytophthora infestans* and *Phytophthora parasitica*, which infect leaves and roots of a broad-spectrum of plants (Kamoun et al., 2015). To achieve

successful infection, these pathogens rely on plant susceptibility genes that facilitate compatibility (van Schie and Takken, 2014; Fawke et al., 2015). Removal of these susceptibility genes has the potential to confer enhanced resistance

(van Schie and Takken, 2014; Fawke et al., 2015). To date, several susceptibility genes to *Phytophthora* pathogens have been reported (Pan et al., 2016; Li et al., 2020; Lu et al., 2020).

We recently found that RNA editing is involved in the regulation of ROS production and immunity (Yang et al., 2020), suggesting that mitochondrial RNA processing and mROS may participate in plant immunity. Here we report the identification of a P-type PPR protein AtRTP7 as a susceptibility factor and a mediator of RNA splicing of *nad7* that encodes one of the core subunits of Complex I. Lack of AtRTP7 also leads to decreased RNA editing levels in *nad1*, *nad3*, and *nad6*, which also encode core subunits of Complex I. We further show that the defective processing of Complex I subunit transcripts in *resistance to P. parasitica 7* (*rtp7*) plants resulted in mROS burst and resistance against a broad spectrum of plant diseases without affecting overall plant development.

## Results

### AtRTP7 is a P-type PPR protein that negatively affects plant immunity to different pathogens

Using the *P. parasitica*–*A. thaliana* compatible interaction system, over ten thousand independent *A. thaliana* T-DNA insertion mutants were previously screened for enhanced resistance to *P. parasitica* (Wang et al., 2011; Pan et al., 2016), leading to the identification of the *rtp7* mutant. AtRTP7 encodes a mitochondria-targeted P-type PPR protein (Narsai et al., 2011) with ten PPR motifs (Figure 1A). We further confirmed its mitochondrial localization by transient co-expression of GFP-tagged AtRTP7 in *Nicotiana benthamiana* leaves with a mitochondrial marker (Figure 1B).

We obtained three T-DNA insertion mutants, *rtp7-1* (SALK\_085606C), *rtp7-2* (SALK\_082825C), and *rtp7-3* (SALK\_029012C) with insertion sites in the first or the second exon of AtRTP7 (Figure 1C). Real-time quantitative PCR (RT-qPCR) analyses showed that the AtRTP7 transcript level was reduced by nearly 100% in *rtp7-1* and *rtp7-3*, but not changed in *rtp7-2* (Supplemental Figure S1). The *rtp7-1* and *rtp7-3* mutants showed enhanced resistance to *P. parasitica*, and the biomass of *P. parasitica* in infected leaves was significantly lower compared with that in Col-0 leaves (Figure 1, D–F).

We next generated transgenic AtRTP7 overexpression (OE) lines in Col-0 background. RT-qPCR analyses showed that AtRTP7 expression levels were significantly upregulated in OE line 5 (OE5) and OE8 (Supplemental Figure S1). In inoculation assays, the OE lines showed enhanced susceptibility to *P. parasitica*, and the biomass of *P. parasitica* in leaves was significantly higher than that in Col-0 leaves (Figure 1, D–F).

We also generated two complementation transgenic lines, comRTP7-1 and comRTP7-2, expressing AtRTP7 under control of its native promoter in *rtp7-1* mutant background. The expression of AtRTP7 in these two complementation lines was significantly recovered as compared to *rtp7-1*

mutant (Supplemental Figure S1). The leaf inoculation assay showed that both comRTP7-1 and comRTP7-2 lines were partially restored to the wild-type disease phenotypes to *P. parasitica* (Figure 1, D and E).

We further tested whether AtRTP7 has similar immune function in plant roots. As the results for leaves, the *rtp7* mutant was more resistant and the OE lines more susceptible to *P. parasitica* (Supplemental Figures S2 and S3). In addition, comRTP7-1 and comRTP7-2 lines were partially restored to the wild-type disease phenotype to *P. parasitica* (Supplemental Figures S2 and S3). RT-qPCR further revealed that AtRTP7 was responsive to *P. parasitica* infection, as it was downregulated during infection (Figure 1G). Taken together, these results suggested that AtRTP7 negatively affects plant immunity to *P. parasitica* in both leaves and roots.

To further examine whether *rtp7* mutants show higher resistance to a broader spectrum of pathogens, we inoculated the leaves of *rtp7-1*, *rtp7-3*, comRTP7-1, comRTP7-2, OE5, OE8, and Col-0 with the bacterial pathogen *Pseudomonas syringae* pv. *tomato* (*Pst*) DC3000, the necrotrophic fungal pathogens *Botrytis cinerea* and *Rhizoctonia solani*, and the oomycete *Phytophthora capsici*. The *rtp7-1* and *rtp7-3* plants showed enhanced resistance to *B. cinerea*, *R. solani*, and *P. capsici*, while the OE5 and OE8 plants were more susceptible (Supplemental Figures S4–S7). In turn, comRTP7-1 and comRTP7-2 lines were partially restored to the wild-type disease phenotypes to these four pathogens (Supplemental Figures S4–S7). However, enhanced resistance of leaves against *Pst* DC3000 (inoculated with  $10^5$  CFU/mL bacteria) was observed in both the *rtp7* mutants and two OE lines as compared with Col-0 at 3-day post-inoculation (dpi; Supplemental Figure S7). Taken together, these results indicated that the *rtp7* mutant showed enhanced resistance to both biotrophic and necrotrophic pathogens.

We additionally observed the growth phenotypes of *rtp7* mutants, comRTP7 lines, and OE lines. None of the *A. thaliana* lines showed any substantial developmental differences as compared to Col-0 when grown in soil. However, *rtp7* mutants produced shorter roots at the early growth stage on plates (Supplemental Figure S8). The root length of comRTP7-1 and comRTP7-2 lines in the early growth stage was partially recovered from the *rtp7-1* mutant (Supplemental Figure S8). The OE5 and OE8 lines did not show difference in root length compared with Col-0 (Supplemental Figure S8). These results suggest that AtRTP7 might affect root growth at early growth stage.

### AtRTP7 participates in RNA splicing of mitochondrial *nad7* gene transcripts

P-type PPR proteins represent an important group of proteins that mediate RNA splicing of mitochondrial genes (Bonen, 2008; Brown et al., 2014). When we amplified the mitochondrial transcripts from *rtp7-1* cDNA using RT-PCR (reverse transcription-polymerase chain reaction) with a limited number of amplification cycles (cycle-limited RT-PCR), we found that the accumulation of fully processed *nad7*

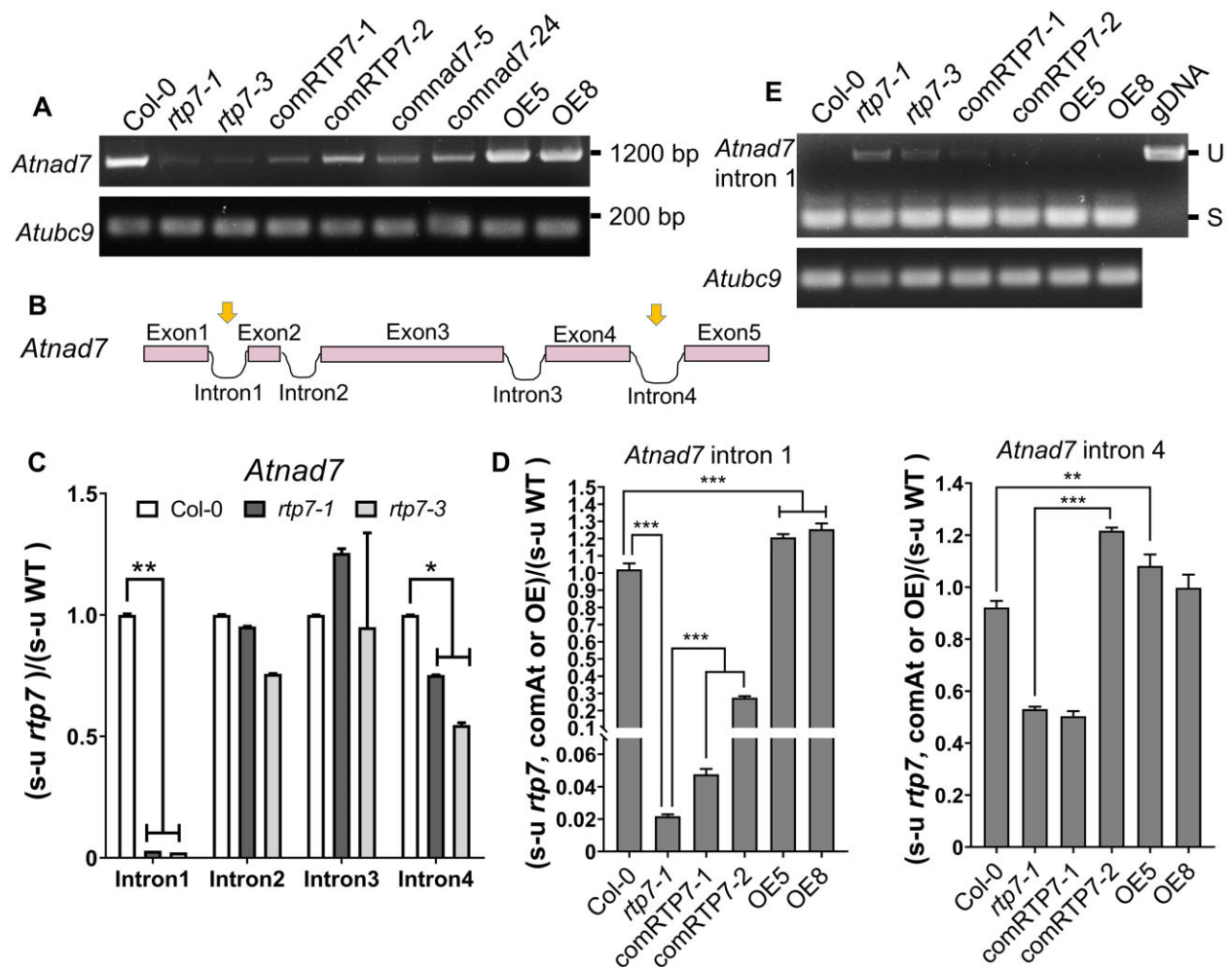


**Figure 2** AtRTP7 participates in RNA splicing of *nad7* in *A. thaliana* mitochondria. A, The results of cycle-limited RT-PCR to detect the levels of fully processed *nad7* transcripts. *Arabidopsis thaliana* UBC9 was used to normalize loading. Fully processed *nad7* transcript is ~1,200 bp. B, A schematic view of the introns and exons of the *nad7* locus. There are five exons and four introns in *nad7*. Arrows indicate the introns whose splicing efficiency was decreased in *rtp7-1* mutant. C and D, RT-qPCR results showing the relative proportions of spliced (s) to unspliced (u) forms of *nad7* introns in *rtp7* mutants (C), comRTP7 lines (D), and OE lines (D). Results are presented as the mean  $\pm$  SE of at least three repeats (three leaves from different plants were collected together as one repeat). Statistical significance was assessed by Student's *t* test. \**P* < 0.05, \*\**P* < 0.01, and \*\*\**P* < 0.001. E, The results of cycle-limited RT-PCR to detect intron 1 spliced (S) or unspliced (U) *nad7* levels. *Arabidopsis thaliana* UBC9 was used to normalize loading. The Col-0 gDNA was used as the marker for the intron 1 unspliced version of *nad7*.

transcripts was clearly lower than that in Col-0 (Figure 2A). We further examined accumulation levels of fully processed *nad7* transcripts in *rtp7* mutants, two OE lines, and two complementation lines by RT-PCR. These results showed that the levels of fully processed *nad7* transcripts were similarly reduced in *rtp7-1* and *rtp7-3* mutant plants (Figure 2A). Furthermore, the levels of fully processed *nad7* transcripts were partially recovered in the two complementation lines (Figure 2A).

Since it has been reported that loss of proper splicing leads to reduced accumulation of fully processed transcripts (Koprivova et al., 2010), and we observed some different sized PCR products in the gel when we amplified the *nad7* transcript by PCR (Supplemental Figure S9), we tested the splicing efficiency of the four introns of *Atnad7* in the leaves of *rtp7-1*, *rtp7-3*, and Col-0 by RT-qPCR. These results

showed a clear impairment in splicing of *nad7* intron 1 and to a lesser extent in splicing of intron 4 in *rtp7-1* and *rtp7-3* (Figure 2, B and C). We further examined the splicing efficiency of *nad7* intron 1 in two OE lines and two complementation lines by RT-qPCR. The splicing efficiencies of *nad7* intron 1 were significantly increased and corresponded to AtRTP7 expression levels in comRTP7-1 and comRTP7-2 as compared to the *rtp7-1* mutant (Figure 2D). Consistent with this, AtRTP7 OE5 and OE8 lines showed a slight but significant increase in the splicing of intron 1 as compared to Col-0 (Figure 2D). These results were further confirmed by RT-PCR-based detection of intron 1 spliced and unspliced versions of *nad7* (Figure 2E). However, when we examined the splicing efficiency of *nad7* intron 4 in OE lines and complementation lines, we found that it was increased in OE5 and OE8 but only significantly in OE5 compared to Col-0.

Among the complementation lines, only comRTP7-2 showed significantly increased splicing efficiency of intron 4 as compared to *rtp7-1* mutant plants by RT-qPCR (Figure 2D). These results suggest that AtRTP7 is involved in the regulation of splicing of *nad7* intron 1 but may also have some functions in the splicing of intron 4.

### *rtp7* mutants show reduced C to U RNA editing levels in *nad1*, *nad3*, and *nad6* gene transcripts

Because many PPR proteins function in C to U RNA editing in mitochondria (Takenaka et al., 2013), we further examined whether AtRTP7 participates in C to U RNA editing. We amplified all transcripts reported to be edited in Arabidopsis mitochondria (Bentolila et al., 2013) by PCR of cDNA synthesized from total RNAs isolated from leaves of the *rtp7-1* and Col-0. DNA sequencing analyses showed that the RNA editing levels were significantly lower at one site in *nad1* (*nad1*-500), two sites in *nad3* (*nad3*-250 and 254) and five sites in *nad6* (*nad6*-103,161,169,191, and 446) in *rtp7-1* mutants as compared to Col-0 (Supplemental Figure S10 and Supplemental Table S1). However, the expression and accumulation of fully processed transcripts of *nad1*, *nad3*, and *nad6* were not significantly different from Col-0 (Supplemental Figure S11, A and B). We further confirmed that the editing extent of these editing sites was also decreased in *rtp7-3* mutant plants (Supplemental Figure S10), whereas the editing extent was restored to wide-type levels in the two complementation lines (Supplemental Figure S10). Loss of editing of these sites would change the secondary structures of the *nad1*, *nad3*, and *nad6* proteins, as predicted by SOPMA ([https://npsa-prabi.ibcp.fr/cgi-bin/npsa\\_automat.pl?page=npsa\\_sopma.html](https://npsa-prabi.ibcp.fr/cgi-bin/npsa_automat.pl?page=npsa_sopma.html)) (Supplemental Figure S11C). These results suggest that knockout of AtRTP7 may have a substantial effect on the function of these proteins.

Although *rtp7-1* mutants showed changes in RNA editing of *nad1*, *nad3*, and *nad6*, the editing extent of these gene transcripts was slightly reduced (Supplemental Figure S10). In contrast, we found that *nad7* transcript levels were strongly reduced in *rtp7* mutants (Figure 2). To further detect whether the RNA editing changes in *rtp7-1* were caused by reduced *nad7* transcript levels, and to further analyze the importance of *nad7* in *rtp7*-mediated plant resistance, we tried to get *nad7* *A. thaliana* mutants. However, *nad7* mutants were unavailable and the generation of knock-out mutants for mitochondrial genes is technically highly challenging. We, therefore, generated transgenic *nad7* complementation lines (comnad7-5 and comnad7-24) in the *rtp7-1* background by expressing fully processed *nad7* transcripts under control of a 35S promoter. To target the nucleus-encoded *nad7* protein to mitochondria, we fused the mitochondrial leading peptide (LP) sequence of *A. thaliana* AOX protein to the N-terminus of the *nad7* protein (Supplemental Figure S12A). We further confirmed that the used AOX LP targeted to mitochondria in *A. thaliana* (Supplemental Figure S12B). The levels of fully processed *nad7* transcripts were clearly increased in the two comnad7

lines as compared to *rtp7* mutants as determined by PCR analysis (Figure 2A). We further amplified *nad1*, *nad3*, and *nad6* from cDNA of comnad7 lines to determine their RNA editing levels. DNA sequencing analyses showed that the RNA editing levels of *nad1*, *nad3*, and *nad6* were significantly restored to Col-0 levels in comnad7 lines (Supplemental Figure S10). These results suggest that the changes of RNA editing extent in these three gene transcripts may be a side effect caused by the low accumulation levels of *nad7* transcripts.

### AtRTP7 regulates plant immunity and salt tolerance through the mitochondrial gene *nad7*

Another PPR protein, BUTHIONINE SULFOXIMINE-INSENSITIVE ROOTS 6 (BIR6, AT3g48250), participates in *nad7* intron 1 splicing, and the *bir6* mutant showed enhanced resistance to oxidative stresses under salt and osmotic stress in *A. thaliana* (Koprivova et al., 2010). Therefore, to further analyze the importance of *nad7* in *rtp7*-mediated phenotypes, we examined whether the *bir6* and *rtp7* mutants had similar phenotypes. We obtained and examined two T-DNA insertion mutants of BIR6, *bir6-4* (SALK\_001888C) and *bir6-5* (SALK\_138713C). RT-qPCR analyses showed that BIR6 expression levels were significantly reduced in both mutants (Supplemental Figure S13). Pathogenicity assays revealed that *bir6* mutants were more resistant to *P. parasitica*, *B. cinerea*, *R. solani*, *P. capsici*, and *Pst* DC3000 (Figure 1; Supplemental Figures S4–S7).

We further examined whether AtRTP7 participated in salinity resistance by 150-mM NaCl treatment of *rtp7* mutants, OE lines, comRTP7 lines. The results showed that *rtp7* mutants also showed enhanced salt resistance as reported for BIR6, and the comRTP7 lines were more sensitive to NaCl treatment than *rtp7-1* mutant plants (Supplemental Figure S14). However, we found that the two AtRTP7 OE lines were also more resistant to salt challenges (Supplemental Figure S14). These results indicate that AtRTP7 and BIR6 share similar functions and may regulate plant immunity through *nad7*.

To further confirm whether *nad7* contributes to the resistance phenotype of *rtp7-1* mutants, we examined comnad7 lines for altered resistance to different pathogens and tolerance to salt tolerance. The results showed that disease resistance to *P. parasitica*, *B. cinerea*, *R. solani*, *P. capsici*, and *Pst* DC3000, and salt tolerance was significantly reduced in comnad7 lines as compared to *rtp7-1* mutant plants (Figure 1; Supplemental Figures S4–S7 and S14). The root length of comnad7-5 and comnad7-24 at early seedling stage was similar to Col-0 (Supplemental Figure S8). These results suggest that disease resistance, salt stress tolerance, and transient developmental phenotypes in *rtp7-1* mutants were mediated by impaired *nad7* intron splicing.

As we found that AtRTP7 had direct effects on splicing of *nad7* intron 1, we tested whether the splicing of *nad7* intron 1 is responsive to *P. parasitica* infection. We, therefore, examined *nad7* splicing efficiencies at eight different infection

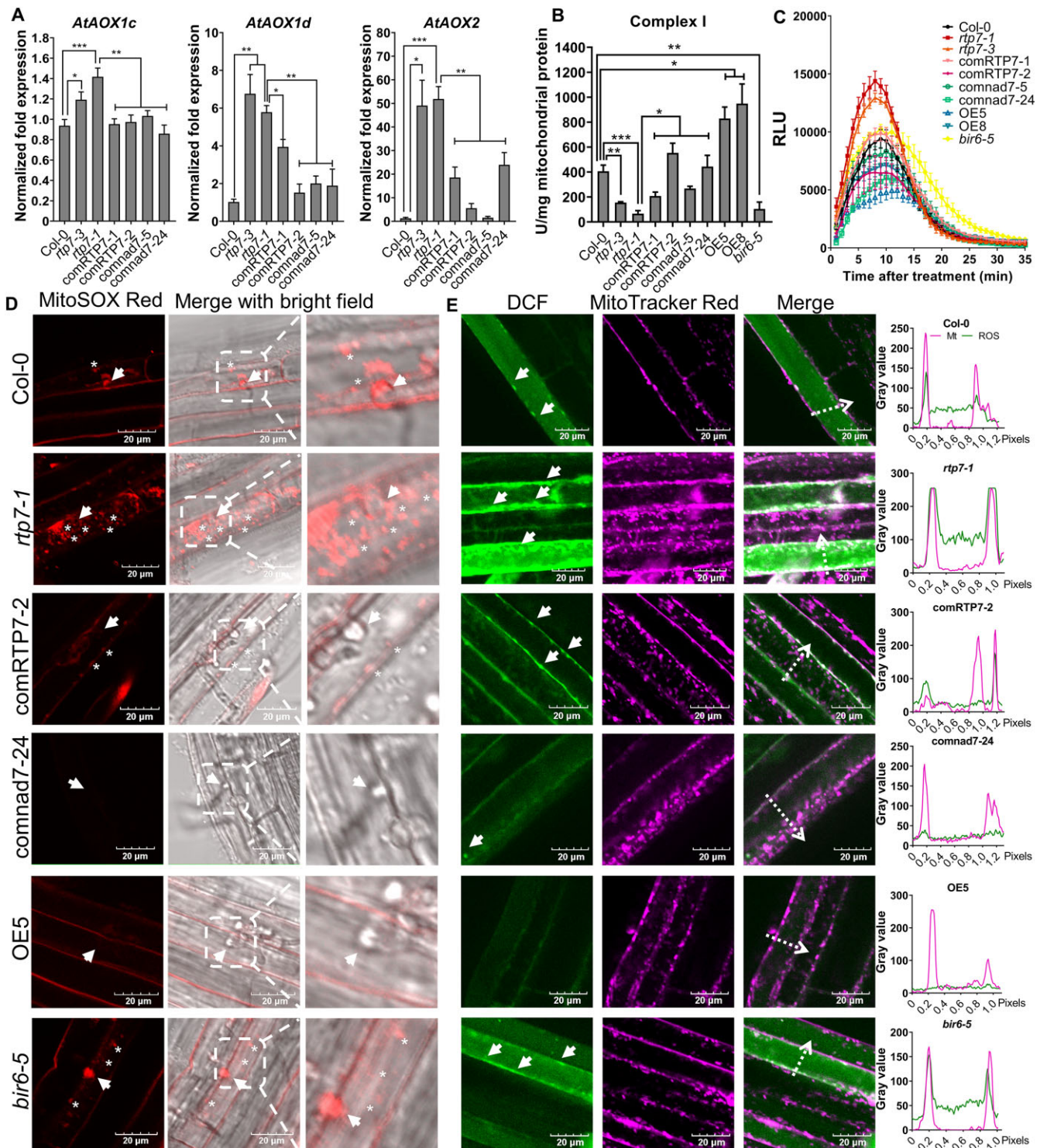


**Figure 3** The *rtp7-1* mutant showed higher mitochondrial ROS levels. **A**, RT-qPCR results showing the expression levels of *AOX1c*, *AOX1d*, and *AOX2* genes. Results are presented as the mean  $\pm$  SE of at least three repeats (two leaves from different plants were gathered together as one repeat). Statistical significance was assessed by Student's *t* test. Similar results were observed in three independent experiments. \**P* < 0.05, \*\**P* < 0.01, and \*\*\**P* < 0.001. **B**, The Complex I activity of *A. thaliana* leaves. The Complex I activity kit (BC0515, Solarbio, Beijing, China) was used for the measurement of the complex I activity in 4-week-old *Arabidopsis* leaves. Results are presented as the mean  $\pm$  SE of at least three repeats (10 to 20 leaves from different plants were gathered together as one repeat). Statistical significance was assessed by Student's *t* test. \**P* < 0.05, \*\**P* < 0.01, and \*\*\**P* < 0.001. **C**, ROS burst in *A. thaliana* leaves treated with 1  $\mu$ M flg22. ROS levels were measured in at least 12 leaves from 6 plants of each group using a luminol-based chemiluminescence assay. Results are presented as the mean  $\pm$  SE of six leaves from different plants. **D**, mROS burst in *A. thaliana* root cells infected with *P. parasitica*, revealed by confocal microscopy observation. *Arabidopsis thaliana* root cells were infected with *P. parasitica* zoospores for  $\sim$ 15 h. The infected roots were stained with 2.5- $\mu$ M MitoSOX Red for 15 min before confocal microscopy

stages postinoculation using RT-qPCR. The analyses showed an increased splicing efficiency of intron 1 during infection (Supplemental Figure S15), suggesting that *nad7* splicing is involved in the *A. thaliana*–*P. parasitica* interaction. We also found that the splicing efficiencies of intron 1 in OE5 and OE8 plants were enhanced as compared to Col-0 during early infection stages, as well as to uninoculated OE5 and OE8 leaves (Supplemental Figure S15), suggesting the increased splicing efficiency of *nad7* may lead to enhanced plant susceptibility to *P. parasitica*.

### The *rtp7-1* mutant shows defects in Complex I activity and higher mitochondrial ROS levels than wild-type

We have found that AtRTP7 is targeted to mitochondria (Figure 1). In addition to chloroplasts (de Torres Zabala et al., 2015), mitochondria are a major ROS production site in cells (Møller, 2001; Huang et al., 2016). In addition, loss of splicing of *nad7* intron 1 was previously reported to severely compromise the function of mitochondrial Complex I (Koprivova et al., 2010), which is one of the major ROS production sites in mitochondria (Møller, 2001; Huang et al., 2016). Since AtRTP7 participates in the splicing of *nad7* and affects RNA editing of some other genes encoding Complex I subunits (Figure 2; Supplemental Figure S10), we wondered whether the activity of Complex I was affected in the *rtp7* mutant. We first used RT-qPCR to examine the transcript levels of AOX (alternative oxidase) family genes whose expressions are usually induced to scavenge mROS in the respiratory ETC mutants, especially in those with Complex I defects (Koprivova et al., 2010). The expressions of *AOX1c*, *AOX1d*, and *AOX2* were induced in the *rtp7-1* and *rtp7-3* mutants as compared to Col-0 (Figure 3A), while their transcript levels were significantly reduced and even reached Col-0 levels in comRTP7 and comnad7 lines (Figure 3A). We further examined the Complex I activity in AtRTP7-related lines. As expected, Complex I activities were significantly reduced in the *rtp7-1* and *rtp7-3* mutants, while the OE lines showed enhanced Complex I activity (Figure 3B) as compared to Col-0, and the comRTP7 and comnad7 lines showed enhanced Complex I activity as compared to *rtp7-1* mutants (Figure 3B). In sum, this series of analyses indicated that the loss of RTP7 resulted in an impaired Complex I activity and probably enhanced mROS production.

To analyze whether *rtp7-1* mutants showed enhanced mROS, we co-labeled *A. thaliana* roots with the ROS fluorescence probe DCF (CM-H<sub>2</sub>DCFDA) and mitochondria

fluorescence marker MitoTracker Red. Microscopic observation showed that only a few mitochondria were stained by DCF in Col-0, whereas more mitochondria were stained with stronger fluorescence in the *rtp7-1* and *rtp7-3* mutant (Supplemental Figure S16A). We also found that *bir6* mutants, which were reported to be reduced with Complex I abundance, were enhanced with mROS, like the *rtp7-1* mutant (Supplemental Figure S16B). The AtRTP7 complementation lines comRTP7-1 and comRTP7-2, and *nad7* complementation lines comnad7-5 and comnad7-24 showed clearly reduced mROS levels as compared to the *rtp7-1* mutant (Supplemental Figure S16C). These results suggest that the AtRTP7 could participate in mROS bursts by affecting Complex I function.

Since ROS play an important role in plant immunity, we further examined whether *rtp7* mutants showed an alteration in immunity-associated ROS burst. We first examined total ROS levels upon treatment with flg22, an elicitor of PAMP-triggered immunity (PTI) by a luminol-based assay. The results showed that upon flg22 treatment, *rtp7-1* and *rtp7-3* leaves exhibited higher ROS levels, while the OE lines showed a reduced ROS burst as compared to Col-0 (Figure 3C). The comRTP7 and comnad7 lines showed a reduced ROS burst as compared with *rtp7-1* mutant leaves (Figure 3C). Similar results were observed when flg22-treated roots were stained with the ROS fluorescence probe DCF (Figure 3E). These results suggest that AtRTP7 is involved in PTI-induced ROS bursts, and the enhanced ROS burst in *rtp7* mutants may be caused by a functionally impaired *nad7* protein. To further analyze the role of ROS burst during *P. parasitica* infection of roots, we inoculated Col-0 and *rtp7-1* roots with *P. parasitica* zoospores and stained them with DCF. The analysis showed that higher ROS signals in *rtp7-1* roots during *P. parasitica* infection as compared to Col-0 (Supplemental Figure S17). These results suggest that AtRTP7 may regulate plant immune responses by affecting ROS levels.

To further examine whether mitochondrial ROS also participate in the flg22-induced ROS burst in *rtp7* mutants, we visualized mROS using DCF and MitoTracker Red staining upon flg22 treatment. flg22 treatment increased the number and fluorescence intensity of mitochondrial ROS signals both in Col-0 and *rtp7-1* mutant plants (Supplemental Figure S18). However, the abundance and fluorescence intensity of DCF-stained mitochondria were higher in *rtp7-1* mutants as compared to Col-0 upon flg22 treatment (Supplemental Figure S18). These results suggest that flg22

#### Figure 3 (Continued)

observation. The arrows and asterisks mark haustoria and mROS, respectively. Two *rtp7* mutants, OE lines, comRTP7 lines, comnad7 lines, and *bir6* mutants were examined and showed similar phenotypes. Similar results were observed in at least three *P. parasitica* infected roots. E, Confocal microscopy observation of mROS in the roots of 10-day-old *A. thaliana* seedlings upon flg22 treatment. The images were taken at 5–8 min after 10- $\mu$ M flg22 treatment. ROS was visualized using the fluorescence probe DCF. Mitochondria were marked using MitoTracker Red. The arrow marks the mROS in root cells. The gray value plots show the relative fluorescence along the dotted line in the images. Two *rtp7* mutants, OE lines, comRTP7 lines, comnad7 lines, and *bir6* mutants were examined and showed similar phenotypes. Similar results were observed in at least three *A. thaliana* roots.



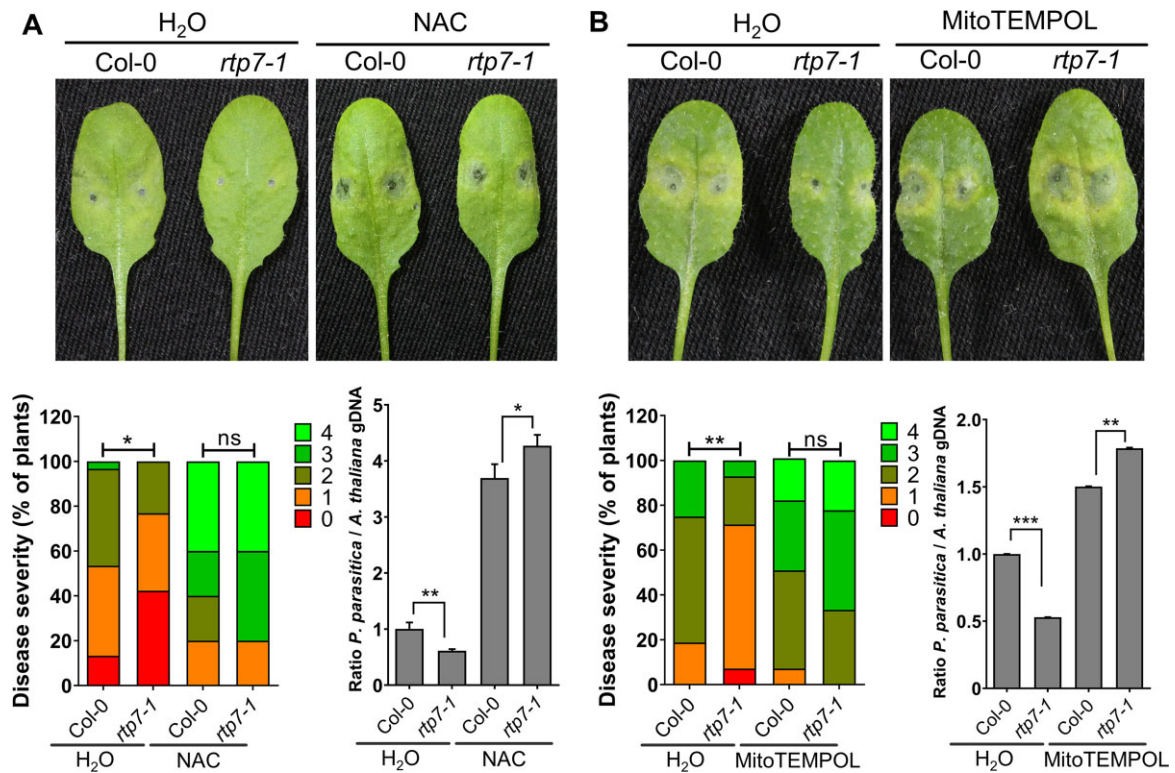


**Figure 4** mROS are required for the enhanced resistance of *A. thaliana rtp7-1* plants to *P. parasitica*. Images, assessment of disease severity of the infected leaves, and quantification of *P. parasitica* biomass after treatment with ROS scavenger NAC (A) or mROS scavenger MitoTEMPOL (B). The leaves of 4-week-old *rtp7-1* and wild-type Col-0 seedlings were treated with 10- $\mu$ g/mL NAC, or 10- $\mu$ M MitoTEMPOL, using water as a mock treatment, followed by inoculation with 2000 *P. parasitica* zoospores. Images were taken at ~24 h (A) or ~48 h (B) postinoculation for the assessment of disease severity of the infected leaves. The statistical significance was assessed by Wilcoxon–Mann–Whitney test. Similar results were observed in three independent experiments. Biomass of *P. parasitica* is shown as the mean  $\pm$  SE of three repeats (two leaves from different plants were collected together as one repeat). Statistical significance was assessed by Student’s *t* test for biomass analysis. \**P* < 0.05, \*\**P* < 0.01, \*\*\**P* < 0.001 and ns, not significant.

activated mROS production. We further compared mROS levels upon flg22 treatments in *rtp7* mutants, AtRTP7 OE, comRTP7, and comnad7 lines. We found that fewer mitochondria were stained by DCF in response to flg22 in the two AtRTP7 OE lines as compared to Col-0 (Figure 3E) and mROS levels were also reduced in the comRTP7 and comnad7 lines as compared to *rtp7-1* mutant plants (Figure 3E). These results indicated that loss of AtRTP7 enhanced PTI-associated mROS bursts, and this phenotype was caused by the absence of nad7.

However, when we tried to analyze the mROS burst in *A. thaliana* root cells during *P. parasitica* infection, we found that the mitochondria could not be labeled by MitoTracker Red in the *P. parasitica* infected cells, which may be caused by changes in normal mitochondrial transmembrane potential ( $\Delta\Psi$ m). To further examine the mROS burst in *P. parasitica*-infected root cells, we inoculated the roots of Col-0, *rtp7* and *bir6-5* mutants, comRTP7, comnad7 and OE lines with *P. parasitica* and stained them with the mROS-specific fluorescence probe MitoSOX Red (Cvetkovska and Vanlerbergh, 2012). The analyses revealed that more mitochondria showed mROS signals in *rtp7* and *bir6-5* as compared to Col-0 during *P. parasitica* infection (Figure 3D). In

the OE lines, there were much less mROS signals as compared to Col-0 root cells (Figure 3D) and mROS signals were reduced in comRTP7 and comnad7 lines as compared to *rtp7-1* mutants (Figure 3D). Taken together, these results indicate that *rtp7* mutant may mediate enhanced plant immunity through mROS.

#### mROS are required for the enhanced resistance of *rtp7-1* to *P. parasitica*

To further investigate the importance of enhanced mROS levels in mediating enhanced resistance of the *rtp7* mutants to *P. parasitica*, we treated *A. thaliana* leaves with the mROS-specific scavenger MitoTEMOPOL or the general ROS scavenger *N*-acetyl-cysteine (NAC) upon inoculation with *P. parasitica* zoospores. MitoTEMPOL is a mitochondrial-targeted free radical scavenger used for mROS depletion (Li et al., 2017; Supinski et al., 2020). NAC is an antioxidant that is widely used for ROS depletion in animal and plant cells (Yao and Greenberg, 2006; Su et al., 2016; Huang et al., 2018). As MitoTEMPOL has not been used for mROS depletion in plant cells, we first confirmed that the MitoTEMPOL could reduce mROS levels in *A. thaliana* (Supplemental Figure S18). We found that the *rtp7* mutant showed

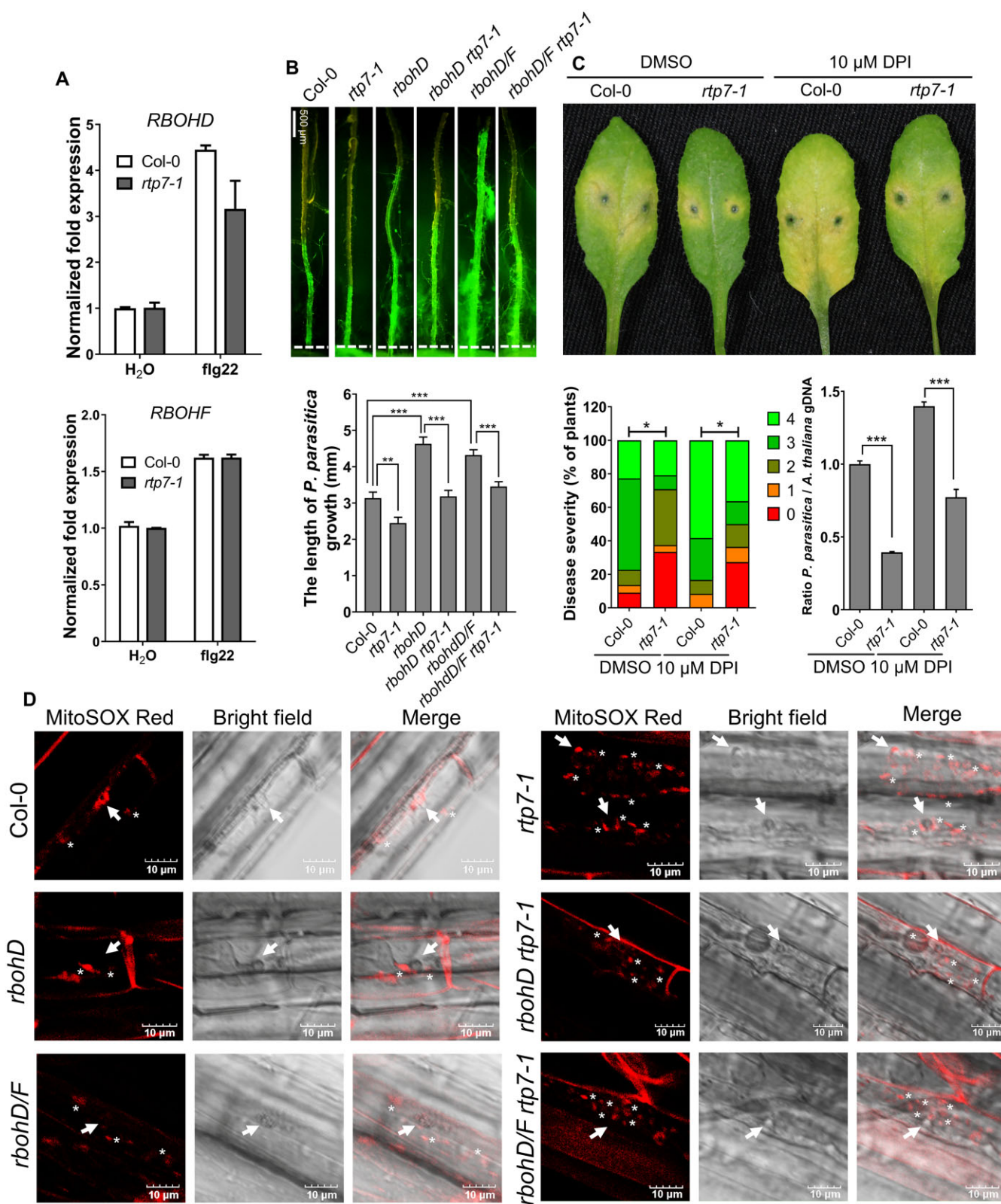


**Figure 5** The enhanced resistance of *rtp7-1* mutant is independent of plasma membrane-localized NADPH oxidases. **A**, The expression levels of *RbohD* and *RbohF* in *rtp7-1* mutant and Col-0 seedlings 1-h post treatment with 10  $\mu$ M flg22. Seedlings were treated with water as a mock control. Five 7-day-old seedlings were collected for each group. Results are presented as the mean  $\pm$  SE of three group. Statistical significance was assessed by Student's *t* test. Similar results were observed in two independent experiments. **B**, The growth of *P. parasitica* hyphae in *A. thaliana* roots. Hyphal growth was measured at 24 hpi. Results are presented as the mean  $\pm$  SE of at least 16 seedlings. Statistical significance was assessed by Student's *t* test. \*\**P* < 0.01 and \*\*\**P* < 0.001. **C**, Images, assessment of disease severity of the infected leaves, and quantification of *P. parasitica* biomass after treatment with DPI. The leaves of 4-week-old *rtp7-1* and wild-type Col-0 seedlings were treated with 10- $\mu$ M DPI, using DMSO as a

significantly enhanced susceptibility to *P. parasitica* after treatment with either NAC or MitoTEMPO as compared to Col-0 (Figure 4). Consistently, we found that Col-0 leaves were also more susceptible to *P. parasitica* upon NAC or MitoTEMPO treatments as compared to the untreated Col-0 leaves (Figure 4). These results suggest that mROS and ROS contribute to the resistance to *P. parasitica* in Col-0 leaves and that the higher levels of mROS and total ROS are required for the enhanced *P. parasitica* resistance in *rtp7* mutants.

### Plasma membrane-localized NADPH oxidases are not the key factors mediating enhanced resistance in *rtp7-1* mutants

Plasma membrane-localized NADPH oxidase encoded by *RBOHD* and *RBOHF* plays important roles in the flg22-induced ROS burst, and their expression is induced by flg22 (Li et al., 2014; Morales et al., 2016). To find out whether the higher ROS levels in the *rtp7-1* mutant occurs along with changes in *RBOHD* or *RBOHF* transcription, we examined their transcript levels by RT-qPCR in the mutant and Col-0 seedlings at 1 h after flg22 treatment. The results showed that the transcript levels of *RBOHD* and *RBOHF* were unchanged in *rtp7-1* mutants as compared to Col-0 (Figure 5A). We also found that the transcript level of *RBOHD* was unchanged during early *P. parasitica* infection stages (Supplemental Figure S19).

To further analyze the importance of *RBOHD* and *RBOHF* in *rtp7*-mediated resistance, we constructed *rbohD rtp7-1* double and *rbohD rbohF rtp7-1* (*rbohD/F rtp7-1*) triple mutants. We compared the immune phenotypes of Col-0, *rtp7-1*, *rbohD*, *rbohD/F*, *rbohD rtp7-1*, and *rbohD/F rtp7-1* mutants by root inoculation with *P. parasitica* zoospores. The analyses indicated that the *rbohD* or *rbohD/F* mutants were more susceptible than Col-0 (Figure 5B). However, the *AtRTP7* mutation further enhanced plant resistance to *P. parasitica* in the *rbohD* or *rbohD/F* background (Figure 5B).

To further examine the role of RBOHs in the immunity of *rtp7-1* plants, we treated Col-0 and *rtp7-1* mutant roots with DPI (Diphenyleneiodonium chloride) to inhibit NADPH oxidase activity (Lohar et al., 2007; Zhang et al., 2014), followed by inoculation with *P. parasitica*. The results showed that after DPI treatment, *rtp7-1* mutant plants remained enhanced resistance to *P. parasitica* compared with Col-0 (Supplemental Figure S20), while the DPI treated Col-0 and *rtp7-1* seedlings were more susceptible compared with

DMSO-treated Col-0 and *rtp7-1* plants (Supplemental Figure S20).

Because the *rbohD/F* double mutants showed growth defects (Supplemental Figure S19), we could not analyze their immune phenotypes to *P. parasitica* on leaves. Therefore, we treated Col-0 and *rtp7-1* mutant leaves with DPI followed by inoculation with *P. parasitica* zoospores. The results were similar to the DPI treatment in roots (Figure 5C). These results suggest that mROS and plasma membrane-produced ROS both contribute to the resistance in *rtp7* mutants, as the DPI treatment of *rtp7* mutants showed enhanced susceptibility compared with untreated *rtp7* mutants and *rbohD* mutation could also increase the susceptibility of *rtp7*. But because the DPI-treated *rtp7* mutants still showed stronger resistance compared to DPI-treated Col-0, and the *rbohD rtp7* and *rbohD/F rtp7* mutants still showed enhanced resistance compared to *rbohD* or *rbohD/F* mutants, suggesting that *RBOHD* and *RBOHF* proteins are not the key factors in mediating *AtRTP7* mutation-induced plant resistance, and the plasma membrane-localized NADPH oxidase-produced ROS may not be necessary for the *rtp7*-mediated resistance.

As *rtp7* mutants showed enhanced mROS levels and mROS are required for the *rtp7*-mediated plant resistance (Figures 3 and 4), to further analyze whether *RBOHD* or *RBOHF* protein is vital to the high mROS levels that were observed in *rtp7* mutants upon flg22 treatment and *P. parasitica* inoculation, we compared mROS levels in Col-0, *rtp7-1*, *rbohD*, *rbohD/F*, *rbohD rtp7-1*, and *rbohD/F rtp7-1* mutants by MitoTracker Red and DCF staining upon flg22 treatment. The analyses showed that the *RBOHD* and *RBOHF* mutations did not inhibit the mROS burst upon flg22 treatment in *rbohD* and *rbohD/F* mutants (Supplemental Figure S21). Furthermore, the *AtRTP7* mutation could enhance mROS levels in the *rbohD* and *rbohD/F* background (Supplemental Figure S21). We also examined mROS levels in roots of all mutants during *P. parasitica* infection by DCF and MitoSOX Red staining. The experiments indicated that *rbohD* and *rbohD/F* mutants had slightly enhanced mROS levels as compared to Col-0 (Figure 5D; Supplemental Figure S21) while the *rbohD rtp7-1* double mutant or *rbohD/F rtp7-1* triple mutant showed enhanced mROS levels as compared to *rbohD* or *rbohD/F* mutants (Figure 5D; Supplemental Figure S21). Taken together, these

### Figure 5 (Continued)

mock treatment, followed by inoculation with 2,000 *P. parasitica* zoospores. Images were taken at ~48 hpi for the assessment of disease severity of the infected leaves. Statistical significance was assessed by Wilcoxon–Mann–Whitney test. Biomass of *P. parasitica* is shown as the mean  $\pm$  SE of three repeats (three leaves from different plants were collected together as one repeat). Statistical significance was assessed by Student's *t* test for biomass analysis. Similar results were observed in three independent experiments. \**P* < 0.05, \*\*\**P* < 0.001. D, mROS burst in *A. thaliana* root cells infected with *P. parasitica*, revealed by confocal microscopy observation. *Arabidopsis thaliana* root cells were infected with *P. parasitica* zoospores for ~15 h. The infected roots were stained with 2.5- $\mu$ M MitoSOX Red for 15 min before confocal microscopy observation. The arrows and asterisks mark haustoria and mROS, respectively. Similar results were observed in at least three *P. parasitica* infected roots.

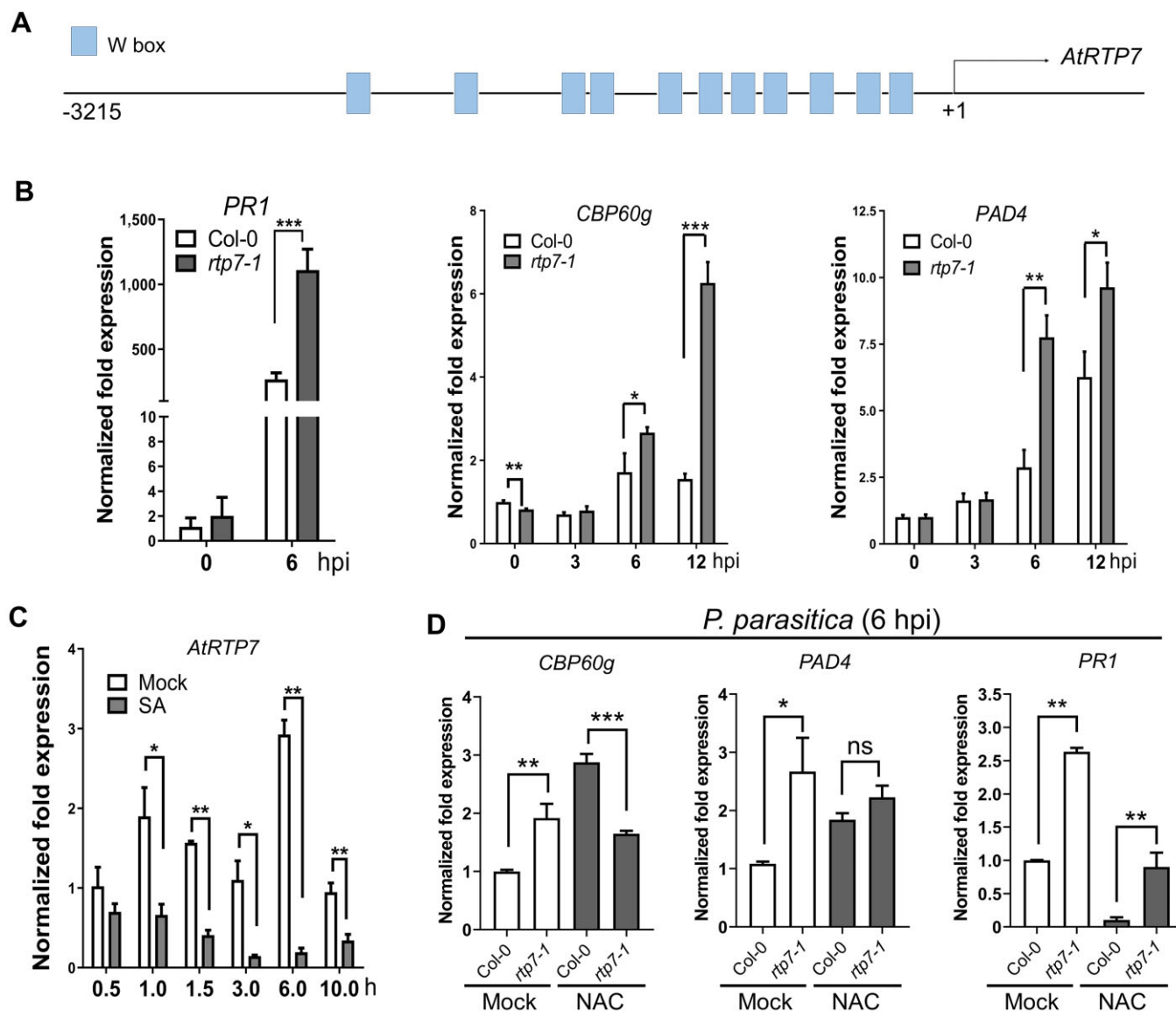


**Figure 6** SA signaling is upregulated in *rtp7-1* mutant plants. **A**, Schematic view of W boxes in the *AtRTP7* promoter. There are 11 predicted W boxes. The cis-elements were predicted using the Plant cis-acting regulatory DNA elements database (<https://www.dna.affrc.go.jp/PLACE/?action=newplace>). **B**, Expression of defense marker genes in the *rtp7-1* mutant and Col-0 at different time points (hpi) during *P. parasitica* infection. The SA signaling pathway marker genes *PR1*, *PAD4*, and *CBP60g* were examined. The *A. thaliana* *UBC9* gene was used as an internal control. Results are presented as the mean  $\pm$  SE of three repeats (three leaves from different plants were collected together as one repeat). Statistical significance was assessed by Student's *t* test. \**P* < 0.05, \*\**P* < 0.01, and \*\*\**P* < 0.001. Similar results were observed in two independent experiments. **C**, The RT-qPCR results for the expression of *AtRTP7* after SA treatment. Results are presented as the mean  $\pm$  SE of three repeats (ten seedlings were collected together as one repeat). Similar results were observed in three independent experiments. Statistical significance was assessed by Student's *t* test. \**P* < 0.05 and \*\**P* < 0.01. **D**, RT-qPCR results showing the expression of *PAD4*, *CBP60g*, and *PR1* in the *rtp7* mutant and Col-0 after NAC treatment at 6-hpi of *P. parasitica* zoospores. Results are presented as the mean  $\pm$  SE of three biological repeats (three leaves from different plants were collected together as one repeat). Statistical significance was assessed by Student's *t* test. \**P* < 0.05, \*\**P* < 0.01, and \*\*\**P* < 0.001.

results suggest that the mROS burst in plant immunity is independent of *RBOHD* and *RBOFH*.

### Salicylic acid signaling is induced in the *rtp7-1* mutant

To investigate the regulation of *AtRTP7* expression, we analyzed the cis-acting elements within the *AtRTP7* promoter. We found that there are 11 W-boxes in the promoter. W-

boxes are potentially bound by WRKY transcription factors and some WRKY proteins play important roles in salicylic acid (SA)-mediated plant defense responses (Bakshi and Oelmüller, 2014) (Figure 6A). Therefore, we examined the expression of *AtRTP7* after SA treatment using RT-qPCR analysis, with results showing that *AtRTP7* was downregulated after SA treatment (Figure 6C). We also examined the expression of SA and jasmonic acid (JA) signaling pathway

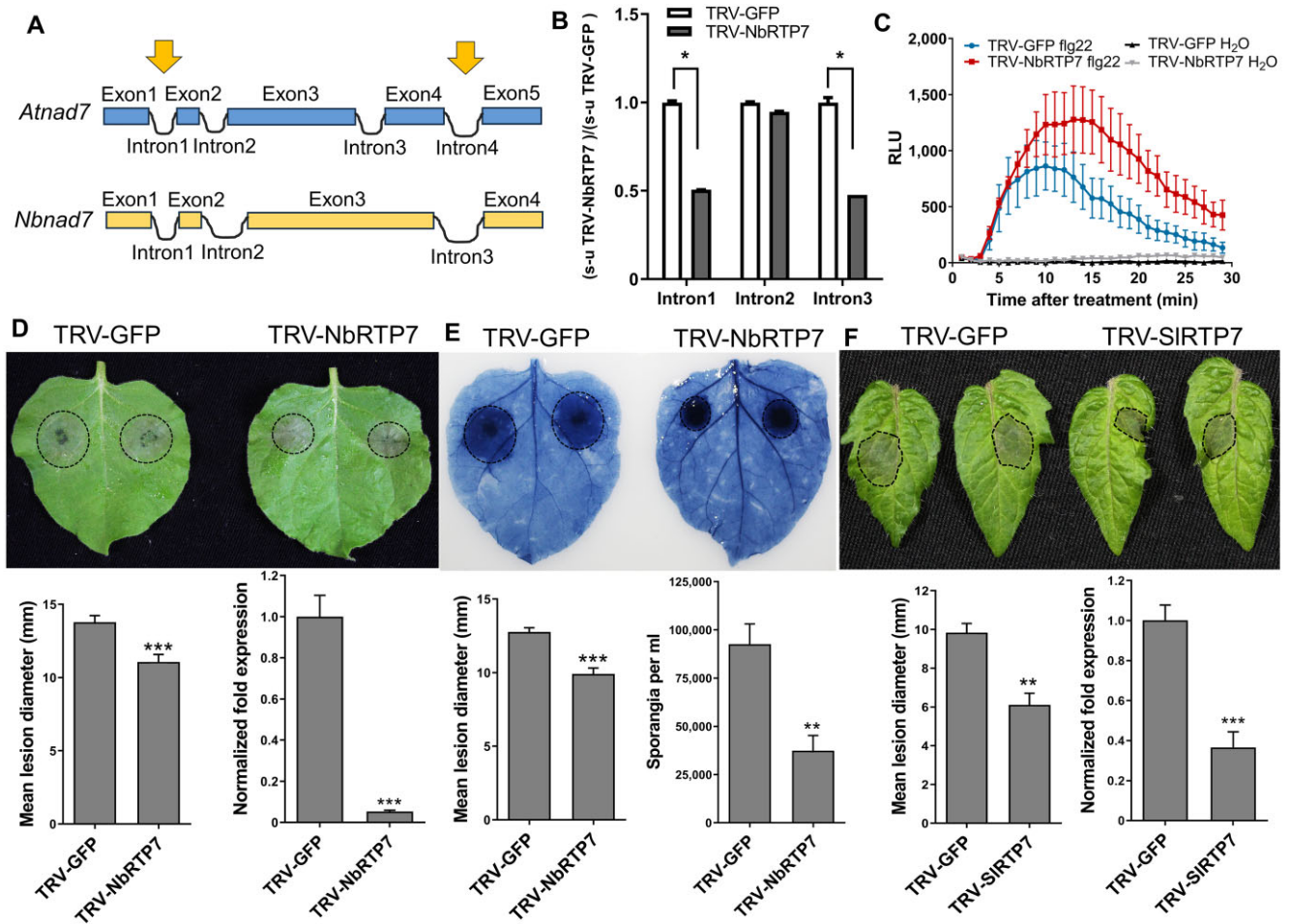


**Figure 7** The immune function of *RTP7* is conserved across distantly related plant species *A. thaliana*, *N. benthamiana*, and *S. lycopersicum*. A, Schematic view of the introns and exons in *Atnad7* and *Nbnad7*. Intron 3 in *A. thaliana* has been lost in *N. benthamiana*. B, RT-qPCR results showing the relative proportions of spliced (s) to unspliced (u) forms of *Nbnad7* introns. Results are presented as the mean  $\pm$ SE of three repeats (three leaves from different plants were collected together as one repeat). Statistical significance was assessed by Student's *t* test. \* $P < 0.05$ . C, ROS burst upon 1- $\mu$ M flg22 treatment in *NbRTP7*-silenced *N. benthamiana*. The relative luminescent unit of at least six leaves from six plants of each group were measured using a luminol-based chemiluminescence assay. Results are presented as the mean  $\pm$ SE of six leaves. D and E, Silencing of *NbRTP7* in *N. benthamiana* led to enhanced resistance to *P. parasitica* (D) and *P. infestans* (E). Images were taken at  $\sim$ 40 h after inoculation with *P. parasitica* zoospores and  $\sim$ 5 days after inoculation with *P. infestans* zoospores. Results for *P. parasitica* lesions are presented as the mean  $\pm$ SE of over 15 lesions from at least 10 leaves. Results for *P. parasitica* lesions are presented as the mean  $\pm$ SE of over 28 lesions from at least 14 leaves. Statistical significance was assessed by Student's *t* test. \*\*\* $P < 0.001$ . Similar results were observed in three independent experiments. RT-qPCR results show the expression of *NbRTP7* in TRV-GFP and TRV-NbRTP7 plants. *Phytophthora infestans* sporangia were collected from TRV-NbRTP7 plants at 10 dpi. Results are presented as the mean  $\pm$ SE of seven leaves. Statistical significance was assessed by Student's *t* test. \*\* $P < 0.01$ . F, *Phytophthora infestans* lesions on *SIRT7*-silenced leaves. Images were taken at  $\sim$ 5 days after inoculation with *P. infestans* zoospores. Results are presented as the mean  $\pm$ SE of five leaves. Statistical significance was assessed by Student's *t* test. \*\*\* $P < 0.001$ . RT-qPCR results show the expression of *SIRT7* in TRV-GFP and TRV-SIRT7 plants. Results are presented as the mean  $\pm$ SE of three repeats (five leaves were collected together as one repeat). The *SIActin* gene was used as an internal control. Similar results were observed in three independent experiments.

marker genes during *P. parasitica* infection of *rtp7-1* and Col-0 leaves. We found that the expression of the SA marker genes *PR1*, *CBP60g*, and *PAD4* was significantly higher in the *rtp7-1* mutant than in Col-0 at 6-h post inoculation (hpi; Figure 6B). The expression of the JA marker gene *PDF1.2* was upregulated in *rtp7-1* without pathogen inoculation (Supplemental Figure S22), but there were no differences in the transcript levels of the JA marker genes *LOX2* and *VSP2* between *rtp7-1* and Col-0 (Supplemental Figure S22). These

results indicate that SA signaling is upregulated in *rtp7-1* and *AtRTP7* expression is downregulated by SA.

To further investigate the importance of higher ROS levels in the activation of SA immune signaling in *rtp7-1* mutant, we quantified *PAD4*, *CBP60g*, and *PR1* expression in NAC-treated Col-0 and *rtp7-1* leaves at 6 hpi with *P. parasitica* zoospores by RT-qPCR. While *PR1* remained higher in *rtp7-1* mutant relative to Col-0, transcript levels of *CBP60g* and *PAD4* were reduced in *rtp7-1* mutants relative to Col-0 after

NAC treatment (Figure 6D). These results suggest that the enhanced expression of *CBP60g* and *PAD4* in *rtp7-1* is dependent on the higher ROS levels.

Because the *rtp7-1* mutant showed an enhanced SA signaling and mROS burst upon flg22 treatment (Figures 3 and 6), we further examined whether AtRTP7 participates in other PAMP-triggered immunity (PTI) responses by measuring flg22-induced callose deposition and the expression of the PTI marker gene *FLG22-INDUCED RECEPTOR-LIKE KINASE 1 (FRK1)* at an early stage of *P. parasitica* infection. The results showed that there was more callose deposition in the *rtp7-1* mutant than in Col-0 after flg22 treatment (Supplemental Figure S23). The transcript level of *FRK1* in *rtp7-1* was higher than that in Col-0 during *P. parasitica* infection (Supplemental Figure S23). These results indicate that the *rtp7* mutant has enhanced PTI responses.

### RTP7 has conserved immune functions across distant plant species

Considering the function of RTP7 in plant immunity, we wondered if RTP7 occurs more widely in the plant kingdom. We identified proteins homologous to AtRTP7 from approximately 100 different plant species in OrthoDB (<https://www.orthodb.org/>). Using these protein sequences, we built a phylogenetic tree and further analyzed the type and position of PPR motifs using MEME suite (<http://meme-suite.org/>). The results showed that RTP7 is conserved and widely found in monocotyledons and dicotyledons (Supplemental Figure S24). We further identified *NbRTP7*, an AtRTP7 ortholog in *N. benthamiana*, and employed virus-induced gene silencing (VIGS) to examine its function in *N. benthamiana*. RT-qPCR assays showed a ~90% reduction in endogenous *NbRTP7* transcripts in *TRV-NbRTP7* plants compared with the *TRV-GFP* control plants (Figure 7D). We confirmed that *NbRTP7* was targeted to mitochondria (Supplemental Figure S25). Because the splicing of the *nad7* intron1 showed the most dramatic change in the *rtp7* mutant, we examined the splicing efficiency of *Nbnad7* in *NbRTP7*-silenced leaves. Unlike *Atnad7*, which has four introns, *Nbnad7* contains three introns and lacks intron 3 of *Atnad7* (Figure 7A). The RT-qPCR assay showed that the splicing of introns 1 and 3 was significantly reduced in the *NbRTP7*-silenced leaves (Figure 7B). The *NbRTP7*-silenced leaves showed an enhanced ROS burst compared with the control leaves (Figure 7C). These results indicate that RTP7 has conserved functions across the distantly related plant species *A. thaliana* and *N. benthamiana*.

To analyze the immune function of *NbRTP7*, we further inoculated *NbRTP7*-silenced leaves with *P. parasitica* or *P. infestans* zoospores. The lesion diameters of *P. parasitica* and *P. infestans* were significantly smaller in *NbRTP7*-silenced leaves compared with the control (Figure 7, D and E). *Phytophthora infestans* sporulation was also significantly reduced (Figure 7E). There were no differences in the growth phenotypes of *NbRTP7*-silenced plants and the *GFP* control plants (Supplemental Figure S26).

We also silenced *SIRTP7* in *Solanum lycopersicum* using VIGS followed by inoculation with *P. infestans*. We obtained similar results to those in *N. benthamiana*: *SIRTP7*-silenced plants showed enhanced resistance to *P. infestans* and did not show changes in growth phenotypes (Figure 7F; Supplemental Figure S26). The RT-qPCR assays showed a ~60% reduction in endogenous transcripts of *SIRTP7* in *TRV-SIRTP7* plants compared with the *TRV-GFP* control plants (Figure 7F). These results indicate that *NbRTP7* and *SIRTP7* have similar immune functions as the orthologous gene in *A. thaliana*, suggesting that the immune function of RTP7 is conserved across distantly related plant species.

### Discussion

Mitochondria play essential roles in primary and energy metabolism in animal and plant cells. The electrochemical gradient established by the ETC is part of oxidative phosphorylation, the main site for the synthesis of ATP and reduction equivalents. The ETC is also a site for mROS production which is an important signaling molecule in immunity and cell death in animals (Chen et al., 2018; Delierneux et al., 2020). Mice and macrophages defective in mROS accumulation show enhanced susceptibility to bacterial and protozoan parasites (West et al., 2011) while high levels of mROS are involved in different cell death programs, including apoptosis and necrosis (Delierneux et al., 2020). Despite the importance of mitochondria for overall cell functionality in eukaryotes as well as in metazoan immunity, our knowledge about mitochondrial processes in plant immunity is very limited.

In this study, we found that the conserved P-type PPR protein RTP7 participates in mitochondrial RNA processing and plant immunity (Figures 1 and 2). AtRTP7 was significantly downregulated in Arabidopsis during infection with the pathogen *P. parasitica* (Figure 1G) and mutants lacking AtRTP7 showed enhanced resistance to *P. parasitica*, and various biotrophic and necrotrophic fungal, oomycete and bacterial pathogens including *P. capsici*, *B. cinerea*, *R. solani*, and *Pst* DC3000 (Figure 1; Supplemental Figures S2–S7). It has been reported that the RNA editing in chloroplast could participate in the plant immunity: *A. thaliana* protein OCP3 functions in the RNA editing of chloroplast gene *ndhB* and further regulates the activity of chloroplast NADH dehydrogenase-like complex (NDH) (Garcia-Andrade et al., 2013). The *ocp3* mutant and mutants lacking the two PPR genes *CRR21* and *CRR2*, which also affect *ndhB* editing, showed enhanced resistance to necrotrophic pathogens *P. cucumerina* and *B. cinerea* (Garcia-Andrade et al., 2013). Recently, one rice (*Oryza sativa*) mitochondrion-localized PPR protein, OsNBL3, was reported to function in RNA splicing of *nad5* intron 4, and its mutants showed enhanced resistance to *Magnaporthe oryzae* and *Xanthomonas oryzae* pv. *oryzae*, as well as salt tolerance (Qiu et al., 2021). Taken all these together, these results suggest that PPR protein may also participate in the regulation of plant immunity by

a fine-tuned regulation of the function of mitochondria or chloroplast complexes.

Although we found that the *rtp7* mutants showed enhanced resistance to a broad spectrum of plant pathogens and salt stress (Figure 1; Supplemental Figures S2–S7 and S14), we noticed that the *AtRTP7* OE lines with reduced ROS levels (Figure 3) also showed enhanced resistance to the bacterial pathogen *Pst* DC3000 and tolerance to salt stress (Supplemental Figures S7 and S14). Attenuating ROS levels by OE of plant AOX genes was reported to enhance resistance to *Pst* DC3000 in *A. thaliana* (Nie et al., 2015). Therefore, the enhanced bacterial resistance in *AtRTP7* OE lines may occur despite low ROS levels. Host plant ROS levels were reported to be crucial for the successful colonization and development of hemibiotrophic pathogens since its proper level is required to regulate cell death during the transition from biotrophic to necrotrophic infection stages (Li et al., 2019a). As *Pst* DC3000 is also a hemibiotrophic pathogen, we presume that low ROS levels in *AtRTP7* OE lines may disturb the transition process during *Pst* DC3000 pathogenesis. It further implies that fine tuning of host ROS levels decides whether the outcome is host resistance or successful infection.

We found that both OE and knockout of *AtRTP7* improved salt stress tolerance in *A. thaliana* (Supplemental Figure S14). Our study further revealed that Complex I activities were reduced in *rtp7* mutants (Figure 3B), which is consistent with reports showing that inhibition of Complex I activity enhanced salt tolerance, though this inhibition induced more ROS production (Koprivova et al., 2010; Sako et al., 2020; Qiu et al., 2021). This reported enhanced salt stress tolerance was thought to be caused by an upregulation of ROS scavenging enzymes, which protected plant cells from the oxidative damage caused by salt treatment (Zhao et al., 2021). At the same time, the salt tolerance could also be conferred by reduced ROS levels as OE of the ROS scavenging enzymes ascorbate peroxidases or glutathione S-transferase enhanced tolerance to salinity in plants (Zhao et al., 2021). Taken together, the enhanced salt tolerance in *AtRTP7* OE lines is likely caused by maintenance of low ROS levels.

Based on our findings, *AtRTP7* participates in RNA splicing of *nad7* and affects the editing of three additional transcripts encoding for subunits of ETC Complex I (Figure 2; Supplemental Figure S10). We found that loss of *AtRTP7* reduced Complex I activity (Figure 3B), which is consistent with previous reports that loss of normal RNA processing of Complex I subunit transcripts leads to reduced mitochondrial Complex I activity (Koprivova et al., 2010; Hammani et al., 2011; Haili et al., 2016; Leu et al., 2016). Furthermore, *rtp7-1* mutants showed reduced sensitivity to Complex I inhibitor rotenone (Supplemental Figure S27). These results suggest that the function of Complex I was impaired in *rtp7-1* mutants. Complex I is an important ROS production site within the mitochondrial ETC (Møller, 2001; Huang et al., 2016), and defects in ETC complexes lead to increased

mROS production (Chen et al., 2018). We found that *rtp7* mutants showed higher levels of mROS production upon flg22 treatment or *P. parasitica* inoculation (Figure 3). Furthermore, treatment of *rtp7-1* mutants with the mROS scavenger MitoTEMPOL abolished *P. parasitica* resistance (Figure 4), indicating that the mROS burst plays an important role in plant immunity of *rtp7-1* mutants. Further analyses showed that plasma membrane-localized RBOHD and RBOHF are not the key factors for the *rtp7*-mediated enhanced resistance, as shown by *P. parasitica* inoculation assays on *rbohD rtp7-1* and *rbohD/F rtp7-1* mutants (Figure 5). Consistently, treatment with RBOHs activity inhibitor DPI did not abolish resistance of *rtp7-1* mutant as compared to DPI treated Col-0 (Figure 5). We further found that *rbohD* and *rbohD/F* mutants did not inhibit mROS burst upon flg22 treatment or *P. parasitica* inoculation (Figure 5; Supplemental Figure S21), suggesting that mROS may represent a ROS burst pathway independent of the well-studied RBOHD/F-dependent plasma membrane ROS burst in plant immunity. Furthermore, MitoTEMPOL treatments also reduced Col-0 resistance to *P. parasitica* (Figure 4), indicating that mROS may also play an important role in plant resistance to pathogens.

In addition to our finding that the mROS levels are increased and essential for the resistance to *P. parasitica* in the *rtp7-1* mutant (Figures 3 and 4), we also found that the total ROS levels were increased in the *rtp7-1* mutant upon flg22 treatment or *P. parasitica* infection (Figure 3; Supplemental Figure S17). And our results indicated that treatment with the ROS scavenger NAC could abolish resistance of the *rtp7-1* mutant to *P. parasitica* (Figure 4). These results indicate that the higher ROS level is important to the resistance of the *rtp7-1* mutant. We also found that when we reduced the mROS levels using MitoTEMPOL, the nonmitochondrial ROS levels were also slightly reduced in the Col-0 upon flg22 treatment, while the reduction was much stronger in the *rtp7-1* mutant (Supplemental Figure S18). In the ROS-induced ROS release (RIRR) pathway in animal cells, the collapse of mitochondrial  $\Delta\Psi_m$  triggers the opening of mitochondrial pores and further releases mROS to the cytosol; during pathogenesis, the mitochondria release a large amount of ROS to cytosol and activate the downstream apoptosis or autophagy pathways (Zandalinas and Mittler, 2018). We found that the mitochondria gather around the haustorial neck with mROS (Supplemental Figure S28), and we detected stronger ROS signals around the whole haustoria in *rtp7-1* mutant (Supplemental Figure S17). It will be interesting to further investigate whether this phenomenon is related to mitochondrial RIRR and whether RIRR exists in plants. It will also be worthwhile to further examine the possible link between mROS and nonmitochondrial ROS signaling in plant, and its function in regulating plant immunity.

In addition to the enhanced mROS levels in *rtp7-1* mutant, we could detect mROS signals around the neck region of *P. parasitica* haustoria in MitoSOX Red stained cells of

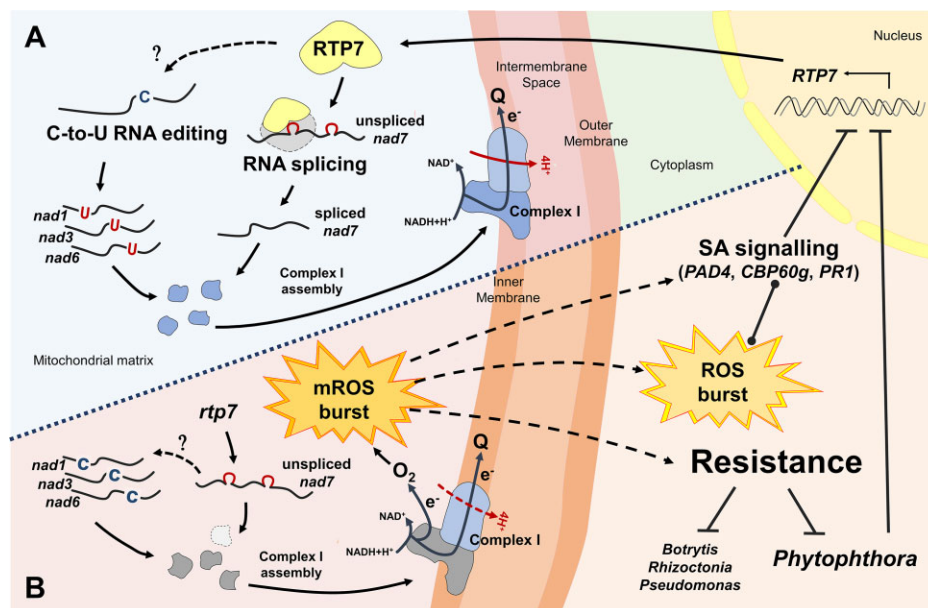


**Figure 8** Schematic model for the role of RTP7 in plant immunity. A, RTP7 is a mitochondrial localized P-Type PPR protein that regulates Complex I assembly of the respiratory chain by mediating intron splicing of *nad7*, and has effect on RNA editing of Complex I subunits *nad1*, *nad3*, and *nad6*. Complex I is responsible for electron transport and generation of a proton gradient. B, *Phytophthora* infection suppresses RTP7 transcription. The resulting absence or reduced abundance of RTP7 protein affects RNA splicing and editing of *nad* mRNAs in mitochondria. Improper RNA processing of Complex I subunits, as observed in *rtp7* mutant plants, results in enhanced mROS and probably total ROS generation. This ROS burst supports plant immunity and associated SA defense and is required for enhanced resistance against plant pathogens as indicated in *rtp7* mutants. The ability of SA treatment to suppress RTP7 transcription might present a positive feedback loop to sustain plant immunity.

Col-0 and *rtp7-1*, although more mitochondria gathered around the haustoria in the *rtp7-1* mutant (Supplemental Figure S28). We further generated transgenic lines with mitochondria-targeted RFP protein in Col-0 and *rtp7-1* background and observed that the number of mitochondria was increased in *rtp7-1* mutants as compared to Col-0 root cells, but slightly smaller in size (Supplemental Figure S29). These results indicate that the mitochondria may respond to *P. parasitica* infection and may produce mROS to restrict infection, which also reminds us of the previous research showing that mitochondria gathered and became immobilized around the fungal invasion sites and showed redox imbalance of the mitochondrial matrix (Fuchs et al., 2016). Our observation also suggests that the accumulation of the mitochondria around the infection sites may be a common plant (immune) response to different pathogens.

In animal liver cells, SA directly interacts with Complex I to induce mROS-mediated apoptosis (Battaglia et al., 2005). We found that SA regulated AtRTP7 expression and SA signaling was activated in *rtp7-1* mutants (Figure 6). Our studies might therefore indicate a role of AtRTP7 in balancing the effect of SA on mitochondria and a potential role of mROS together with SA in plant immunity regulation. The higher expression levels of SA signaling markers *PAD4* and *CBP60g* observed in our study were dependent on the higher ROS levels in *rtp7-1* mutant (Figure 6), suggesting a possible link between mROS and SA signaling.

Homologs of AtRTP7 with RNA splicing capabilities of *nad7* are widely found in monocotyledonous and dicotyledonous plants (Supplemental Figure S24). The *Nicotiana sylvestris nad7* mutant was reported to show increased tolerance to Tobacco mosaic virus (Dutilleul et al., 2003). BIR6 functions in *nad7* splicing, and we found that *bir6* mutants also enhanced with mROS and resistance to *P. parasitica* (Figure 1; Supplemental Figures S2 and S3). We also found that the *nad7* complementation lines, in the *rtp7-1* background, restored the resistance and mROS levels of *rtp7-1* mutant to Col-0 level (Figure 1; Supplemental Figures S2 and S3). These results indicate that AtRTP7 and BIR6 participate in immune responses (e.g. mROS production) in *A. thaliana* through the regulation of ETC component *nad7*. The atomic structure of mitochondrial Complex I of *A. thaliana* was recently reported, using cryo-electron microscopy (Klusck et al., 2021). The data showed that all *nad* genes (*nad1*, *nad2*, *nad3*, *nad4*, *nad4L*, *nad5*, *nad6*, *nad7*, and *nad9*) in the mitochondrial genome encode core subunits of Complex I (Klusck et al., 2021). Among the nine *nad* proteins, *nad7* contains three FeS clusters: N6a, N6b, and N2 (Klusck et al., 2021), and the N2 FeS cluster donates electrons directly to ubiquinone (Hameedi et al., 2021), suggesting the potential key function of the *nad7* subunit in electron transfer.

The *nad7* protein is highly conserved between *A. thaliana* and Solanaceae plants (Supplemental Figure S30). The conservation of RTP7 and *nad7* suggests that RTP7 may have similar functions in different plant species. We did observe



that NbRTP7 functions in the splicing of *Nbnad7* introns 1 and 3, and that NbRTP7-silenced plants are increased with ROS burst like that in the *rtp7* mutant (Figure 7). We further found that NbRTP7-silenced *N. benthamiana* and SIRT7-silenced *S. lycopersicum* plants both were enhanced with resistance to *P. infestans* (Figure 7). These results suggest that RTP7 may have a conserved immune function across distant plant species. Importantly, unlike the dwarf and late flowering phenotypes of some Complex I mutants (Dutilleul et al., 2003; Koprivova et al., 2010), *rtp7* plants did not show a significant changes in growth and development phenotype (Supplemental Figure S8), suggesting RTP7 as a potential trait for targeted breeding for broad-spectrum disease resistance in different crop species.

In summary, we identified the P-type PPR protein RTP7 as an RNA processing factor of ETC Complex I subunit transcripts and loss of RTP7 functionality led to enhanced plant immunity to broad-spectrum pathogens through increased mROS burst without affecting overall plant development (Figure 8). Our results indicate that the numerous PPR proteins that widely exist in land plants may play important roles in plant immunity.

## Materials and methods

### Plasmid constructs

For the *A. thaliana* RTP7 OE construct, full length *AtRTP7* (At4g02820) was amplified from Col-0 cDNA and cloned into the Xba1 and Xho1 sites of the pKannibal vector (Wesley et al., 2001). To avoid changing the normal targeting of *AtRTP7* to mitochondria, GFP was fused between the mitochondria LP and the rest of RTP7 protein using overlapping PCR and cloned into the Xba1 and Xho1 sites of the pKannibal vector. Then the constructs were digested by Not1, and the resulting fragment containing *AtRTP7* was inserted into pART27 (Gleave, 1992). For the *AtRTP7* complementation construct, full-length *AtRTP7* was amplified from Col-0 cDNA and the native promoter region (2,315 bp) was amplified from Col-0 DNA and cloned into pMDC162 vector. For the *Atnad7* complementation construct, the fully processed *nad7* was amplified from Col-0 cDNA. The LP sequence of Arabidopsis AOX protein was amplified from Col-0 cDNA and these two parts were fused together using overlapping PCR and cloned into pMDC32 vector with Asc1 and Spe1 sites. For VIGS of RTP7 in *N. benthamiana*, a ~300-bp-specific fragment of *NbRTP7* was chosen and amplified from *N. benthamiana* cDNA. For VIGS of RTP7 in *S. lycopersicum*, a ~400-bp-specific fragment of *SIRT7* was chosen and amplified from *S. lycopersicum* cDNA. The PCR products were digested by EcoR1 and Xho1 and inserted into pTRV2. All the primers we used are listed in Supplemental Table S2.

### *Arabidopsis thaliana* transformation and plant growth conditions

The T-DNA insertion lines *rtp7-1* (SALK\_085606C), *rtp7-2* (SALK\_082825C), *rtp7-3* (SALK\_029012C), *bir6-4* (SALK\_001888C), *bir6-5* (SALK\_138713C), and *rbohD*

(SALK\_109396C) were obtained from the Arabidopsis Biological Resource Center. The homozygous *rtp7* or *bir6* lines were confirmed by PCR. All the transgenic lines of *A. thaliana* were generated using the floral dip method (Zhang et al., 2006) and screened on half-strength Murashige and Skoog (1/2 MS) plates with the appropriate antibiotics. The plates were cultured in a growth chamber at 23°C with 5,000 Lx, 16-h light/8-h dark. *Arabidopsis thaliana*, *N. benthamiana*, and *S. lycopersicum* plants were grown in a mixture of vermiculite and nutritive soil (1:2) at 23°C with 60-70% relative humidity and grown under a culture condition (5000 Lx with LED lamps (OUTRACE, OU016-U4B), 11-h light/13-h dark).

### VIGS in *N. benthamiana* and *S. lycopersicum*

VIGS in *N. benthamiana* was performed as previously described (Senthil-Kumar and Mysore, 2014). *Agrobacterium tumefaciens* strain GV3101 containing pTRV1, pTRV2-NbRTP7, pTRV2-GFP, or pTRV2-PDS was grown for 36 h in LB medium with appropriate antibiotics at 28°C. The bacteria were pelleted and resuspended with infiltration buffer (10-mM MES, 10-mM MgCl<sub>2</sub>, and 200-mM acetosyringone). Bacteria harboring pTRV1 and those harboring pTRV2-NbRTP7, pTRV2-GFP, or pTRV2-PDS were mixed in a 1:1 ratio, and the final OD<sub>600</sub> (optical density at 600 nm) for each strain was adjusted to 0.25. The co-cultures were infiltrated into 4-week-old *N. benthamiana* leaves. VIGS in *S. lycopersicum* was performed as previously described (Wang et al., 2015). The final OD<sub>600</sub> for each strain was adjusted to 1.8. The co-cultures were infiltrated into the cotyledons of 1-week-old *S. lycopersicum* seedlings. The plants were grown for 2 more weeks before being used for assays.

### Confocal microscopy

*Arabidopsis thaliana* roots were stained with 100- or 200-nM MitoTracker Red CM-H<sub>2</sub>XROS or MitoTracker Green FM for 1 h to mark mitochondria and 10 μM DCF to detect ROS, then washed twice before imaging. MitoTracker Red was imaged using an excitation wavelength of 561 nm with emission collected at 570–670 nm. MitoTracker Green was imaged using an excitation wavelength of 488 nm with emission collected at 500–540 nm. DCF was excited at 488 nm with emission collected at 500–540 nm. For the MitoSOX Red staining, the infected roots were stained with 2.5-μM MitoSOX Red for 15 min before confocal microscopy observation. MitoSOX Red was excited at 510 nm with emission collected at 570–670 nm.

Any confocal microscopy observations in this study were conducted at least two times with at least three independent plant materials (*A. thaliana* roots or *N. benthamiana* leaves derived from different plants) each time. All the confocal images were taken with at least two authors being present and all people confirmed the phenotypes.

### Pathogen infection assay

GFP-tagged *P. parasitica* strain Pp016, *P. infestans* strain 88069, *P. capsici* strain LT263 and *R. solani* strain AG3pt

isolate HBZJ-5x were used for plant infection. Pathogens were cultured and inoculated as in previous reports (Wang et al., 2011, 2013; Li et al., 2019b): plants were inoculated with 2,000 zoospores for *P. parasitica*, 1,200 for *P. infestans*, and 800 for *P. capsici*. *Phytophthora infestans* sporangia counts were performed as described previously (McLellan et al., 2013; Boevink et al., 2016). *Phytophthora parasitica* infected leaves were observed using a fluorescence microscope with the 4× objective lens and 10× eyepiece. The infected leaves were divided into five categories according to the infection area ratio: grade 0: no infection, grade 1: lesion radius < 1/4 radius of the view field, grade 2: 1/4 radius of the view field < lesion radius < 1/2 radius of the view field, grade 3: 1/2 radius of the view field < lesion radius < full view field, and grade 4: the lesion radius exceeds the radius of the view field. For the NAC treatment during *P. parasitica* infection, the inoculated leaves were observed using a fluorescence microscope with the 5× objective lens and 10× eyepiece. For *P. parasitica* inoculation of *A. thaliana* roots, 7- to 10-day-old seedlings were transferred from 1/2 MS plates to vertical plates containing 1/2 MS medium without sucrose and the roots were inoculated with 0.785 cm<sup>2</sup> GFP-tagged *P. parasitica* mycelium plugs and cultured for 14 days. The elongation of the *P. parasitica* hyphae were observed and photographed using a fluorescence microscope with the 4× objective lens and 10× eyepiece 24 hpi. The length of the hyphae in roots was measured with ImageJ. And the infection phenotype of leaves in seedlings was observed at 14 dpi.

*Pseudomonas syringae* pv. *tomato* (*Pst*) DC3000 was cultured and inoculated as described previously (Pan et al., 2016). *Botrytis cinerea* was cultured and inoculated as described previously (Govrin and Levine, 2002). For *R. solani* inoculation, 10-day-old *A. thaliana* seedlings were transferred from 1/2 MS plates to vertical plates containing 1/2 MS medium without sucrose and the roots were inoculated with 0.785 cm<sup>2</sup> mycelium plugs and cultured for 13 days. The infection phenotype was observed at 4–5 dpi.

### Gene expression assay

Total RNA of plants was extracted using TRIzol reagent (Invitrogen, Waltham, MA, USA), and 800-ng total RNA was reverse-transcribed into cDNA using the PrimeScript RT Reagent Kit with gDNA Eraser (Perfect Real Time) (TakaRa, Kusatsu, Japan). RT-qPCR was performed using FastStart Universal SYBR Green Master (ROX) (Roche, Basel, Switzerland) with specific primers in a LightCycler 480 (Roche, Basel, Switzerland). The relative gene expression level was calculated using the  $2^{-\Delta\Delta C_t}$  method with the house-keeping gene *PpActin* as the reference for *P. parasitica*, *AtUBC9* for *A. thaliana*, *EF1 $\alpha$*  for *N. benthamiana*, and *SIActin* for *S. lycopersicum*. For cycle-limited RT-PCR, the target genes were amplified for 27 cycles using EasyTaq DNA polymerase (TransGen Biotech, Beijing, China). All the primers are listed in Supplemental Data Set 1.

### RNA editing assay

To analyze the extent of RNA editing in mitochondria, RNA was isolated from *A. thaliana* leaves and reverse-transcribed into cDNA using the PrimeScript RT Reagent Kit with gDNA Eraser (Perfect Real Time) (TakaRa, Kusatsu, Japan). The mitochondria genes were amplified with specific primers and then sequenced. The cDNA sequences were evaluated for C to T differences at the RNA editing sites. The extent of editing was estimated by measuring the relative heights of the respective nucleotide peaks.

### Phylogenetic analysis

For phylogenetic analysis, protein sequences of AtRTP7 and its orthologs were downloaded from the Arabidopsis Information Resource (<http://www.arabidopsis.org/>) and OrthoDB (<https://www.orthodb.org/>). The alignment and phylogenetic analysis were performed using MEGA7 with default parameters (Kumar et al., 2016). The neighbor-joining method with 1,000 bootstrap replicates was used. The position of the PPR motif in AtRTP7 was obtained from UniProt (<https://www.uniprot.org/>), and the PPR motifs of the AtRTP7 orthologs were identified using MEME suite (<http://meme-suite.org/>). The tree was annotated using Evolview (<https://www.evolgenius.info/>). The alignments used for phylogenetic analysis are provided as Supplemental Files S1 and S2.

### ROS burst detection

ROS production was measured using a luminol-based assay as described previously (Sang and Macho, 2017). Four- to five-week-old *A. thaliana* leaves were sliced into 0.5 mm<sup>2</sup> discs and floated in water overnight. Water was replaced with reagent containing luminol, peroxidase, and 1  $\mu$ M flg22. ROS released by the leaf discs was measured by detecting the luminescence of luminol.

### Salt treatment

Four-day-old *rtp7-1* and Col-0 seedlings were transferred from 1/2 MS plates to vertical plates containing 1/2 MS medium with or without 150-mM NaCl. The seedlings were cultured vertically for 7 days. The seedlings were imaged every day, and ImageJ was used to measure the root length until the seventh day after salt treatment. The fresh weight of seedlings was measured at the seventh day after salt treatment.

### Statistical analysis

The data for gene expression, lesion diameter, biomass, plant height, and root length obtained from most experiments were analyzed using Student's *t* test. The cell death and disease severity assessment assays were analyzed using Wilcoxon–Mann–Whitney test. All the statistical analyses were performed by SSPS. \**P* < 0.05. \*\**P* < 0.01. \*\*\**P* < 0.001. Data for statistical analyses are provided as Supplemental Data Set 2.

## Accession numbers

Genes described here in have the following The Arabidopsis Information Resource (<https://www.arabidopsis.org/>) gene accession numbers: *AtRTP7* (AT4G02820), *AtBIR6* (AT3G48250), *RBOHD* (AT5G47910), *RBOHF* (AT1G64060), *Atnad7* (ATMG00510). *NbRTP7* (Niben101Scf00317g06017.1), and *SIRTP7* (Solyc06g005140.3.1) in Sol Genomics Network (<https://solgenomics.net/>).

## Supplemental data

The following materials are available in the online version of this article.

**Supplemental Figure S1.** The expression levels of *AtRTP7* in *rtp7* mutants, comRTP7 lines, and OE lines.

**Supplemental Figure S2.** The growth of *P. parasitica* hyphae in *A. thaliana* roots.

**Supplemental Figure S3.** *AtRTP7* negatively affects plant immunity to *P. parasitica* in roots.

**Supplemental Figure S4.** *AtRTP7* negatively affects plant resistance to *B. cinerea*.

**Supplemental Figure S5.** *AtRTP7* negatively affects root resistance to *R. solani*.

**Supplemental Figure S6.** *AtRTP7* negatively affects plant resistance to *P. capsici*.

**Supplemental Figure S7.** Quantification of *Pst* DC3000 growth in *A. thaliana*.

**Supplemental Figure S8.** The growth phenotype of *rtp7* mutants.

**Supplemental Figure S9.** The electrophoresis of *nad7* PCR products in *rtp7-1* mutant.

**Supplemental Figure S10.** *rtp7* mutants showed reduced C to U RNA editing levels of *nad1*, *nad3* and *nad6*.

**Supplemental Figure S11.** Loss of editing may change the secondary structures of *nad1*, *nad3*, and *nad6* in the *rtp7* mutants.

**Supplemental Figure S12.** MtLP-RFP is localized in mitochondria in *A. thaliana*.

**Supplemental Figure S13.** The expression levels of *BIR6* in *bir6* mutants.

**Supplemental Figure S14.** The *rtp7-1* mutant showed enhanced tolerance to salt.

**Supplemental Figure S15.** The splicing efficiency of *nad7* intron 1 was enhanced in *A. thaliana* during *P. parasitica* infection.

**Supplemental Figure S16.** mROS levels of *A. thaliana* root cells.

**Supplemental Figure S17.** The *rtp7* mutant showed stronger ROS burst than that in the Col-0 root cells infected with *P. parasitica*, as revealed by confocal microscopy observation.

**Supplemental Figure S18.** MitoTEMPOL could reduce the mROS burst in the *rtp7-1* mutant upon flg22 treatment.

**Supplemental Figure S19.** The growth phenotypes of *rbohD/F* and *rbohD/F rtp7-1* mutants.

**Supplemental Figure S20.** The growth of *P. parasitica* hyphae in *rtp7-1* and Col-0 roots upon DPI treatment.

**Supplemental Figure S21.** mROS burst in *rbohD*, *rbohD rtp7-1*, *rbohD/F*, and *rbohD/F rtp7-1* root cells revealed by confocal microscopy observation.

**Supplemental Figure S22.** The JA signaling pathway marker gene *PDF1.2* was upregulated in the *rtp7* mutant but not the expression of *LOX2* and *VSP2*.

**Supplemental Figure S23.** The callose deposition and the expression of the PTI marker gene *FRK1* were increased in the *rtp7* mutant.

**Supplemental Figure S24.** A phylogenetic tree of RTP7 in monocotyledons and dicotyledons.

**Supplemental Figure S25.** LP-GFP-NbRTP7 localized in the mitochondria.

**Supplemental Figure S26.** Growth phenotypes of *NbRTP7*-silenced and *SIRTP7*-silenced plants.

**Supplemental Figure S27.** The rotenone treatment of *rtp7-1* mutant and Col-0.

**Supplemental Figure S28.** Mitochondria were accumulated around the haustoria of *P. parasitica*.

**Supplemental Figure S29.** *rtp7* mutants showed increased number of mitochondria.

**Supplemental Figure S30.** NAD7 is conserved in *A. thaliana*, *Nicotiana* species, and Solanaceae plants.

**Supplemental Table S1.** Effect of *rtp7-1* mutant in mitochondrial C to U RNA editing.

**Supplemental Data Set 1.** List of primers used in the study.

**Supplemental Data Set 2.** The results of statistical tests in this study.

**Supplemental File S1.** Alignments used to generate phylogenetic trees.

**Supplemental File S2.** Phylogenetic trees of RTP7.

## Acknowledgments

We thank Dr Gary J. Loake (University of Edinburgh, UK), Dr Stefan Binder (Ulm University, Germany), Dr Ruth Schäfer (Ulm University, Germany), Dr Guangjin Fan (Southwest University, China), and all the lab members for their insightful suggestions and encouragement. We thank Dr Meixiang Zhang (Shaanxi Normal University, China) for the *rbohD/F* double mutant seeds, and Ms Yan Li and Ms Zhenzhen Ma (Northwest A&F University, China) for technical support in confocal microscopy.

## Funding

This work was supported by China Agriculture Research System (CARS-09), the National Natural Science Foundation of China (#31125022 and #31930094), and the Program of Introducing Talents of Innovative Discipline to Universities (project 111) from the State of Administration for Foreign Experts Affairs, PR China (#B18042).

**Conflict of interest statement.** A patent based on this study has been filed by Northwest A&F University with W.S. and Y.Y. as inventors.

## References

- Amirsadeghi S, Robson CA, Vanlerberghe GC** (2007) The role of the mitochondrion in plant responses to biotic stress. *Physiol Plant* **129**: 253–266
- Bakshi M, Oelmüller R** (2014) WRKY transcription factors: Jack of many trades in plants. *Plant Signal Behav* **9**: e27700
- Barkan A, Small I** (2014) Pentatricopeptide repeat proteins in plants. *Annu Rev Plant Biol* **65**: 415–442
- Battaglia V, Salvi M, Toninello A** (2005) Oxidative stress is responsible for mitochondrial permeability transition induction by salicylate in liver mitochondria. *J Biol Chem* **280**: 33864–33872
- Bentolila S, Oh J, Hanson MR, Bukowski R** (2013) Comprehensive high-resolution analysis of the role of an Arabidopsis gene family in RNA editing. *PLoS Genet* **9**: e1003584
- Boevink PC, Wang X, McLellan H, He Q, Naqvi S, Armstrong MR, Zhang W, Hein I, Gilroy EM, Tian Z, et al.** (2016) A *Phytophthora infestans* RXLR effector targets plant PP1c isoforms that promote late blight disease. *Nat Commun* **7**: 10311
- Bonen L** (2008) *Cis*- and *trans*-splicing of group II introns in plant mitochondria. *Mitochondrion* **8**: 26–34
- Braun HP, Binder S, Brennicke A, Eubel H, Fernie AR, Finkemeier I, Klodmann J, König AC, Kuhn K, Meyer E, et al.** (2014) The life of plant mitochondrial complex I. *Mitochondrion* **19** (Pt B): 295–313
- Brown GG, Colas des Francs-Small C, Ostersetzer-Biran O** (2014) Group II intron splicing factors in plant mitochondria. *Front Plant Sci* **5**: 35
- Chandel NS** (2014) Mitochondria as signaling organelles. *BMC Biol* **12**: 34
- Chen Y, Zhou Z, Min W** (2018) Mitochondria, oxidative stress and innate immunity. *Front Physiol* **9**: 1487
- Colombatti F, Gonzalez DH, Welchen E** (2014) Plant mitochondria under pathogen attack: a sigh of relief or a last breath? *Mitochondrion* **19** (Pt B): 238–244
- Cvetkovska M, Vanlerberghe GC** (2012) Coordination of a mitochondrial superoxide burst during the hypersensitive response to bacterial pathogen in *Nicotiana tabacum*. *Plant Cell Environ* **35**: 1121–1136
- de Torres Zabala M, Littlejohn G, Jayaraman S, Studholme D, Bailey T, Lawson T, Tillich M, Licht D, Bolter B, Delfino L, et al.** (2015) Chloroplasts play a central role in plant defence and are targeted by pathogen effectors. *Nat Plants* **1**: 15074
- Delierneux C, Kouba S, Shanmughapriya S, Potier-Cartereau M, Trebak M, Hempel N** (2020) Mitochondrial calcium regulation of redox signaling in cancer. *Cells* **9**: 432
- Dutilleul C, Garmier M, Noctor G, Mathieu C, Chétrit P, Foyer CH, de Paeppe R** (2003) Leaf mitochondria modulate whole cell redox homeostasis, set antioxidant capacity, and determine stress resistance through altered signaling and diurnal regulation. *Plant Cell* **15**: 1212–1226
- Fawke S, Doumane M, Schornack S** (2015) Oomycete interactions with plants: infection strategies and resistance principles. *Microbiol Mol Biol Rev* **79**: 263–280
- Fuchs R, Kopschke M, Klapprodt C, Hause G, Meyer AJ, Schwarzlander M, Fricker MD, Lipka V** (2016) Immobilized subpopulations of leaf epidermal mitochondria mediate PENETRATION2-dependent pathogen entry control in Arabidopsis. *Plant Cell* **28**: 130–145
- García-Andrade J, Ramirez V, Lopez A, Vera P** (2013) Mediated plastid RNA editing in plant immunity. *PLoS Pathog* **9**: e1003713
- Gleave AP** (1992) A versatile binary vector system with a T-DNA organisational structure conducive to efficient integration of cloned DNA into the plant genome. *Plant Mol Biol* **20**: 1203–1207
- Govrin EM, Levine A** (2002) Infection of *Arabidopsis* with a necrotrophic pathogen, *Botrytis cinerea*, elicits various defense responses but does not induce systemic acquired resistance (SAR). *Plant Mol Biol* **48**: 267–376
- Gray MW, Covello PS** (1993) RNA editing in plant mitochondria and chloroplasts. *FASEB J* **7**: 64–71
- Haili N, Planchard N, Arnal N, Quadrado M, Vrielynck N, Dahan J, des Francs-Small CC, Mireau H** (2016) The MTL1 pentatricopeptide repeat protein is required for both translation and splicing of the mitochondrial NADH DEHYDROGENASE SUBUNIT7 mRNA in Arabidopsis. *Plant Physiol* **170**: 354–366
- Hameedi MA, Grba DN, Richardson KH, Jones AJY, Song W, Roessler MM, Wright JJ, Hirst J** (2021) A conserved arginine residue is critical for stabilizing the N2 FeS cluster in mitochondrial complex I. *J Biol Chem* **296**: 100474
- Hammani K, des Francs-Small CC, Takenaka M, Tanz SK, Okuda K, Shikanai T, Brennicke A, Small I** (2011) The pentatricopeptide repeat protein OTP87 is essential for RNA editing of *nad7* and *atp1* transcripts in Arabidopsis mitochondria. *J Biol Chem* **286**: 21361–21371
- Huang S, Van Aken O, Schwarzlander M, Belt K, Millar AH** (2016) The roles of mitochondrial reactive oxygen species in cellular signaling and stress response in plants. *Plant Physiol* **171**: 1551–1559
- Huang Y, Zhang Y, Gao C, Li Z, Guan Y, Hu W, Hu J** (2018) The interactions of plant growth regulators and H<sub>2</sub>O<sub>2</sub> during germination improvement of sweet corn seed through spermidine application. *Plant Growth Regul* **85**: 15–26
- Huang Y, Chen X, Liu Y, Roth C, Copeland C, McFarlane HE, Huang S, Lipka V, Wiermer M, Li X** (2013) Mitochondrial AtPAM16 is required for plant survival and the negative regulation of plant immunity. *Nat Commun* **4**: 2558
- Kamoun S, Furzer O, Jones JD, Judelson HS, Ali GS, Dalio RJ, Roy SG, Schena L, Zambounis A, Panabieres F, et al.** (2015) The top 10 oomycete pathogens in molecular plant pathology. *Mol Plant Pathol* **16**: 413–434
- Klusck N, Senkler J, Yildiz O, Kuhlbrandt W, Braun HP** (2021) A ferredoxin bridge connects the two arms of plant mitochondrial complex I. *Plant Cell* **33**: 2072–2091
- Koprivova A, des Francs-Small CC, Calder G, Mugford ST, Tanz S, Lee BR, Zechmann B, Small I, Kopriva S** (2010) Identification of a pentatricopeptide repeat protein implicated in splicing of intron 1 of mitochondrial *nad7* transcripts. *J Biol Chem* **285**: 32192–32199
- Kumar S, Stecher G, Tamura K** (2016) MEGA7: molecular evolutionary genetics analysis version 7.0 for bigger datasets. *Mol Biol Evol* **33**: 1870–1874
- Leu KC, Hsieh MH, Wang HJ, Hsieh HL, Jauh GY** (2016) Distinct role of *Arabidopsis* mitochondrial P-type pentatricopeptide repeat protein-modulating editing protein, PPME, in *nad1* RNA editing. *RNA Biol* **13**: 593–604
- Li L, Li M, Yu L, Zhou Z, Liang X, Liu Z, Cai G, Gao L, Zhang X, Wang Y, et al.** (2014) The FLS2-associated kinase BIK1 directly phosphorylates the NADPH oxidase BbohD to control plant immunity. *Cell Host Microbe* **15**: 329–338
- Li Q, Ai G, Shen D, Zou F, Wang J, Bai T, Chen Y, Li S, Zhang M, Jing M, et al.** (2019a) A *Phytophthora capsici* effector targets ACD11 binding partners that regulate ROS-mediated defense response in *Arabidopsis thaliana*. *Mol Plant* **12**: 565–581
- Li T, Wang Q, Feng R, Li L, Ding L, Fan G, Li W, Du Y, Zhang M, Huang G, et al.** (2019b) Negative regulators of plant immunity derived from cinnamyl alcohol dehydrogenases are targeted by multiple *Phytophthora* Avr3a-like effectors. *New Phytol* doi: 10.1111/nph.16139 (August 22, 2019)
- Li W, Zhao D, Dong J, Kong X, Zhang Q, Li T, Meng Y, Shan W** (2020) AtRTP5 negatively regulates plant resistance to *Phytophthora* pathogens by modulating the biosynthesis of endogenous jasmonic acid and salicylic acid. *Mol Plant Pathol* **21**: 95–108
- Li Y, Wang Y, Xue H, Pritchard HW, Wang X.** (2017) Changes in the mitochondrial protein profile due to ROS eruption during ageing of elm (*Ulmus pumila* L.) seeds. *Plant Physiol Biochem* **114**: 72–87

- Lohar DP, Haridas S, Gantt JS, VandenBosch KA (2007) A transient decrease in reactive oxygen species in roots leads to root hair deformation in the legume-rhizobia symbiosis. *New Phytol* **173**: 39–49
- Lu W, Deng F, Jia J, Chen X, Li J, Wen Q, Li T, Meng Y, Shan W (2020) The *Arabidopsis thaliana* gene *AtERF019* negatively regulates plant resistance to *Phytophthora parasitica* by suppressing PAMP-triggered immunity. *Mol Plant Pathol* **21**: 1179–1193
- McLellan H, Boevink PC, Armstrong MR, Pritchard L, Gomez S, Morales J, Whisson SC, Beynon JL, Birch PR (2013) An RxLR effector from *Phytophthora infestans* prevents re-localisation of two plant NAC transcription factors from the endoplasmic reticulum to the nucleus. *PLoS Pathog* **9**: e1003670
- Meyer EH, Welchen E, Carrie C (2019) Assembly of the complexes of the oxidative phosphorylation system in land plant mitochondria. *Annu Rev Plant Biol* **70**: 23–50
- Møller IM (2001) Plant mitochondria and oxidative stress: electron transport, NADPH turnover, and metabolism of reactive oxygen species. *Annu Rev Plant Physiol Plant Mol Biol* **52**: 561–592
- Morales J, Kadota Y, Zipfel C, Molina A, Torres MA (2016) The *Arabidopsis* NADPH oxidases *RbohD* and *RbohF* display differential expression patterns and contributions during plant immunity. *J. Exp. Bot.* **67**: 1663–1676
- Narsai R, Law SR, Carrie C, Xu L, Whelan J (2011) In-depth temporal transcriptome profiling reveals a crucial developmental switch with roles for RNA processing and organelle metabolism that are essential for germination in *Arabidopsis*. *Plant Physiol* **157**: 1342–1362
- Nie S, Yue H, Zhou J, Xing D (2015) Mitochondrial-derived reactive oxygen species play a vital role in the salicylic acid signaling pathway in *Arabidopsis thaliana*. *PLoS One* **10**: e0119853
- Pan Q, Cui B, Deng F, Quan J, Loake GJ, Shan W (2016) *RTP1* encodes a novel endoplasmic reticulum (ER)-localized protein in *Arabidopsis* and negatively regulates resistance against biotrophic pathogens. *New Phytol* **209**: 1641–1654
- Qiu T, Zhao X, Feng H, Qi L, Yang J, Peng YL, Zhao W (2021) OsNBL3, a mitochondrion-localized pentatricopeptide repeat protein, is involved in splicing *nad5* intron 4 and its disruption causes lesion mimic phenotype with enhanced resistance to biotic and abiotic stresses. *Plant Biotechnol J* **19**: 2277–2290
- Sako K, Futamura Y, Shimizu T, Matsui A, Hirano H, Kondoh Y, Muroi M, Aono H, Tanaka M, Honda K, et al. (2020) Inhibition of mitochondrial complex I by the novel compound FSL0260 enhances high salinity-stress tolerance in *Arabidopsis thaliana*. *Sci Rep* **10**: 8691
- Sang Y, Macho AP (2017) Analysis of PAMP-triggered ROS burst in plant immunity. *Methods Mol Biol* **1578**: 143–153
- Senthil-Kumar M, Mysore KS (2014) Tobacco rattle virus-based virus-induced gene silencing in *Nicotiana benthamiana*. *Nat Protoc* **9**: 1549–1562
- Serrano I, Audran C, Rivas S (2016) Chloroplasts at work during plant innate immunity. *J Exp Bot* **67**: 3845–3854
- Shikanai T (2015) RNA editing in plants: machinery and flexibility of site recognition. *Biochim Biophys Acta Bioenerg* **1847**: 779–785
- Su L, Lan Q, Pritchard HW, Xue H, Wang X (2016) Reactive oxygen species induced by cold stratification promote germination of *Hedysarum scoparium* seeds. *Plant Physiol Biochem* **109**: 406–415
- Supinski GS, Wang L, Schroder EA, Callahan LAP (2020) MitoTEMPOL, a mitochondrial targeted antioxidant, prevents sepsis induced diaphragm dysfunction. *Am J Physiol Lung Cell Mol Physiol* **319**: L228–L238
- Takenaka M, Zehrmann A, Verbitskiy D, Hartel B, Brennicke A (2013) RNA editing in plants and its evolution. *Annu Rev Genet* **47**: 335–352
- Unsel M, Marienfeld JR, Brandt P, Brennicke A (1997) The mitochondrial genome of *Arabidopsis thaliana* contains 57 genes in 366,924 nucleotides. *Nat Genet* **15**: 57–61
- van Schie CC, Takken FL (2014) Susceptibility genes 101: how to be a good host. *Annu Rev Phytopathol* **52**: 551–581
- Wang T, Wen LW, Zhu HL (2015) Effectively organ-specific virus induced gene silencing in tomato plant. *J Nat Sci* **1**: 31–34
- Wang Y, Bouwmeester K, van de Mortel JE, Shan W, Govers F (2013) A novel *Arabidopsis*-oomycete pathosystem: differential interactions with *Phytophthora capsici* reveal a role for camalexin, indole glucosinolates and salicylic acid in defence. *Plant Cell Environ* **36**: 1192–1203
- Wang Y, Meng Y, Zhang M, Tong X, Wang Q, Sun Y, Quan J, Govers F, Shan W (2011) Infection of *Arabidopsis thaliana* by *Phytophthora parasitica* and identification of variation in host specificity. *Mol Plant Pathol* **12**: 187–201
- Wesley SV, Helliwell CA, Smith NA, Wang MB, Rouse DT, Liu Q, Gooding PS, Singh SP, Abbott D, Stoutjesdijk PA, et al. (2001) Construct design for efficient, effective and high-throughput gene silencing in plants. *Plant J* **27**: 581–590
- West AP, Shadel GS, Ghosh S (2011) Mitochondria in innate immune responses. *Nat Rev Immunol* **11**: 389–402
- Yan J, Zhang Q, Yin P (2017) RNA editing machinery in plant organelles. *Sci China Life Sci* **61**: 162–169
- Yang Y, Fan G, Zhao Y, Wen Q, Wu P, Meng Y, Shan W (2020) Cytidine-to-Uridine RNA editing factor NbMORF8 negatively regulates plant immunity to *Phytophthora* pathogens. *Plant Physiol* **184**: 2182–2198
- Yao N, Greenberg JT (2006) *Arabidopsis* ACCELERATED CELL DEATH2 modulates programmed cell death. *Plant Cell* **18**: 397–411
- Zandalinas SI, Mittler R (2018) ROS-induced ROS release in plant and animal cells. *Free Radic Biol Med* **122**: 21–27
- Zhang C, Bousquet A, Harris JM (2014) Abscisic acid and lateral root organ defective/NUMEROUS INFECTIONS AND POLYPHENOLICS modulate root elongation via reactive oxygen species in *Medicago truncatula*. *Plant Physiol* **166**: 644–658
- Zhang X, Henriques R, Lin SS, Niu QW, Chua NH (2006) *Agrobacterium*-mediated transformation of *Arabidopsis thaliana* using the floral dip method. *Nat Protoc* **1**: 641–646
- Zhao S, Zhang Q, Liu M, Zhou H, Ma C, Wang P (2021) Regulation of plant responses to salt stress. *Int J Mol Sci* **22**: 4609
- Zhu Q, Dugardeyn J, Zhang C, Muhlenbock P, Eastmond PJ, Valcke R, De Coninck B, Oden S, Karampelias M, Cammue BP, et al. (2014) The *Arabidopsis thaliana* RNA editing factor SLO2, which affects the mitochondrial electron transport chain, participates in multiple stress and hormone responses. *Mol Plant* **7**: 290–310